**Articles in PresS. J Neurophysiol (July 10, 2013). doi:10.1152/jn.00232.2013**

**Title:** Dynamic modulation of spike-timing dependent calcium influx during cortico-striatal upstates

**Authors:** Evans RC[1]; Maniar YM[2]; Blackwell KT[1]*

**Affiliations:**

[1]George Mason University, The Krasnow Institute for Advanced Studies, MS 2A1, Fairfax, VA 22030-444, USA

[2]Thomas Jefferson High School for Science and Technology, Alexandria, VA

*corresponding author (kblackw1@gmu.edu)

**Running Head:** Calcium influx during striatal upstates

**Key Words:** striatum, calcium, computational model, medium spiny neuron, upstates

**Word Count:** 7,544

**Conflict of Interest**: The authors have no conflicts of interest

**Acknowledgments:**

We thank John Reynolds for providing traces of *in vivo* upstates and Sriram Damodaran and Wonryull Koh for feedback on earlier versions of this manuscript. This work was supported by NRSA 1F31NS066645 - 01A2 from NINDS awarded to Rebekah Evans and by the ONR grant MURI N00014-10-1-0198

## Abstract

The striatum of the basal ganglia demonstrates distinctive upstate and downstate membrane potential oscillations during slow wave sleep and under anesthetic. The upstates generate calcium transients in the dendrites and the amplitude of these calcium transients depends strongly on the timing of the action potential (AP) within the upstate. Calcium is essential for synaptic plasticity in the striatum and these large calcium transients during the upstates may control which synapses undergo plastic changes. To investigate the mechanisms which underlie the relationship between calcium and AP timing, we have developed a realistic biophysical model of a medium spiny neuron (MSN). We have implemented sophisticated calcium dynamics including calcium diffusion, buffering, and pump extrusion which accurately replicates published data. Using this model, we found that either the slow inactivation of dendritic sodium channels (NaSI) or the calcium inactivation of voltage gated calcium channels (CDI) can cause high calcium corresponding to early APs and lower calcium corresponding to later APs. We find that only CDI can account for the experimental observation that sensitivity to AP timing is dependent on NMDA receptors. Additional simulations demonstrate a mechanism by which MSNs can dynamically modulate their sensitivity to AP timing, and show that sensitivity to specifically timed pre and post-synaptic pairings (as in STDP protocols) is altered by the timing of the pairing within the upstate. These findings have implications for synaptic plasticity *in vivo* during sleep when the upstate-downstate pattern is prominent in the striatum.

## Introduction

Medium spiny neurons (MSNs) are the sole projection neurons of the striatum and plasticity changes in these neurons underlie motor learning (Yin et al., 2009). *In vivo*, the MSNs exhibit distinct membrane potential oscillations referred to as upstates and downstates. Although this upstate-downstate activity pattern was observed more than 30 years ago (Wilson and Groves, 1981), its function is still unclear. This pattern of activity is displayed in anesthetized animals and occurs during slow wave sleep, but is much less prominent in the awake animal (Mahon et al., 2006). Because this activity pattern occurs most strongly when the animal is anesthetized or sleeping and consequently motionless, its main function is not likely

the direct control of motor output. Rather it may be a means to consolidate and reinforce motor skill learning by controlling which specific synapses are strengthened during sleep (Stoetzner et al., 2010) while cells replay previous wakeful sequences (Ribeiro et al., 2004; Lansink et al., 2009).

Large dendritic calcium transients coincide with the cortico-striatal upstate (Kerr and Plenz, 2002, 2004), and calcium elevations are necessary for striatal synaptic plasticity *in vitro* (Fino et al., 2010). Therefore, during the upstate the calcium elevation in the dendrite may dictate whether specific synapses are potentiated or depressed. The timing of the action potential (AP) within the upstate strongly determines the amplitude of the corresponding calcium elevation. APs early in the upstate coincide with higher calcium peaks than APs late in the upstate, resulting in a non-linear, timing-dependent relationship (Kerr and Plenz, 2004). However, the intracellular mechanisms responsible for this relationship and the consequences for synaptic plasticity during the upstate are as yet unknown.

*In vitro* experiments have shown that carefully timed pairings of pre and post-synaptic activity can result in spike timing dependent plasticity (STDP) (Fino et al., 2005; Pawlak and Kerr, 2008), and computational models have demonstrated that calcium influx strongly predicts plasticity during these protocols (Evans et al., 2012). However, the noisy *in vivo* environment is very different from the quiet *in vitro* slice preparation. Specifically, a rigidly controlled single pairing of pre and post synaptic activity is not likely to occur *in vivo*. Instead, barrages of synaptic activity and an underlying upstate-downstate pattern characterize the *in vivo* situation. In this study, we investigate the calcium influx due to STDP pairings during these *in vivo* like upstates and discuss the consequences for synaptic plasticity.

Using a multi-channel, multi-compartmental biophysical model and a sophisticated model of calcium diffusion, buffering, and pump extrusion, we investigate two possible mechanisms which can control the relationship between calcium and AP timing during the upstate. In the first half of the paper, we determine that one mechanism is more likely, and confirm its plausibility with voltage clamp experiments. In the second half of the paper, we use the model to make several experimentally testable predictions. Specifically, we show that AP

timing affects calcium binding to downstream targets involved in plasticity, and demonstrate a mechanism by which MSNs could dynamically modulate their sensitivity to AP timing in response to neuromodulation.

## Methods

*General MSN model.* Using GENESIS simulation software, we developed a model MSN with realistic electrophysiological activity (figure 1) and calcium dynamics (figure 2) by modifying our previously published dorsal striatum MSN (Evans et al., 2012). The morphology is similar (figure 1A), but the maximal dendritic length is reduced to 224µm, and the long tertiary branches slightly taper from 0.8µm to 0.7µm in diameter (figure 1A). These changes are in accordance with reconstructions of MSNs from the NeuroMorpho.org neuronal reconstruction database (Halavi et al., 2008). For simplicity, this model does not contain dendritic spines except where noted for the STDP simulations.

*Ionic channels.* This model contains one fast sodium channel (Naf) (Ogata and Tatebayashi, 1990) and four voltage-gated potassium channels: a fast potassium A current (Kaf, Kv4.2) (Tkatch et al., 2000), a slow potassium A current (Kas, Kv1.2) (Shen et al., 2004), a resistant persistent potassium current (Krp) (Nisenbaum and Wilson, 1995), and an inwardly rectifying potassium current (Kir) (Steephen and Manchanda, 2009). The model also contains two calcium activated potassium channels: the big conductance BK channel and the small conductance SK channel. All equations governing the kinetics of these channels are in appendix tables 1 & 2. Intrinsic channel time constants in this model have been temperature corrected with a qfactor of 3 except Kaf and Naf which are adjusted by a qfactor of 1.5 and 2.5 respectively. BK and SK are not in appendix tables 1&2 as they are the same as in our previous model (Evans et al., 2012). All channels are present in the soma and in the dendrites; however, the maximal conductances of the Naf, Kaf, and Kas channels were adjusted differentially in the soma and dendrites during model tuning (see appendix table 3). Under the sodium slow inactivation (NaSI) conditions, an additional slow inactivation term is added to the dendritic sodium channels (Ogata and Tatebayashi, 1990; Migliore, 1996).

*Calcium channels.* Five voltage gated calcium channels (VGCCs) are included in this model. High voltage activated channels include CaR (Foehring et al., 2000; Brevi et al., 2001), CaN (Cav2.2) (Kasai and Neher, 1992; Bargas et al., 1994; McNaughton and Randall, 1997), and CaL1.2 (Cav1.2) (Kasai and Neher, 1992; Bargas et al., 1994; Wolf et al., 2005; Tuckwell, 2012). Low voltage activated channels include CaT (Cav3.3, α1G) (McRory et al., 2001) and CaL1.3 (Cav1.3) (Wolf et al., 2005; Tuckwell, 2012). Calcium channel kinetics and equations are in appendix tables 1 & 2. For each calcium channel, the Goldman-Hodgkin-Katz (GHK) formula is applied to accurately compute the driving potential for these channels. Under the calcium dependent inactivation (CDI) conditions, an additional calcium-dependent inactivation term is added to the R-type, N-type, and both L-type calcium channels (Liang et al., 2003). The maximal permeabilities of these VGCCs were adjusted in the soma to produce calcium elevations comparable in size and shape to published experiments (Kerr and Plenz, 2002). Similarly, calcium permeabilities in the dendrites were adjusted to match their contributions during back-propagating action potentials (Carter and Sabatini, 2004) (figure 2). Permeabilities are shown in appendix table 3.

*Calcium diffusion, buffers, and pumps.* Calcium dynamics were implemented using the calcium *difshell* object in GENESIS, which integrates changes to calcium concentration produced by calcium influx, buffers, pumps and diffusion. A thin (0.1μm) submembrane shell was created as the outermost shell and concentric shells progressively doubling in thickness were added within the compartment (figure 2A). One dimensional calcium diffusion between shells occurred at a rate of 200$\mu m^2$/sec (Allbritton et al., 1992). Calcium extrusion was achieved by the addition of a Michaelis-Menten pump with km=0.3e-3mM, and Kcat=85pmol/($cm^2$/s) in the soma and 12pmol/($cm^2$/s) in the dendrites. The endogenous calcium buffers calbindin and calmodulin (both N and C terminal binding site) were included with concentrations and kinetics taken from published models (Kim et al., 2010; Oliveira et al., 2012) (Appendix table 4).

*Synaptic channels.* AMPA, NMDA, and GABA receptors are distributed along the dendrites. For simplicity, there is one excitatory synapse (containing AMPA and NMDA) and one inhibitory (GABA) synapse per isopotential compartment. The maximal conductances and time constants

are summarized in appendix table 5. All synaptic channels use the *facsynchan* object in GENESIS, which uses equation 1 to calculate the conductance of the channel from the activation and inactivation time constants ($\tau_1$ and $\tau_2$ respectively), time t relative to the action potential, and the maximal conductance ($g_{max}$). K is a normalization constant which is calculated from the time constants and allows $G_{syn}$ to reach a peak value of $g_{max}$.

(1) $$Gsyn(t) = (K * wt * gmax/\ (\tau_1 - \ \tau_2))(e^{-\frac{t}{\tau 1}} - e^{-\frac{t}{\tau 2}})$$

*wt* = synaptic weight which depends on short term facilitation or depression of these synapses.

(2) $$wt = wt_0 * \frac{1}{1+depr}$$

where $wt_0 = 1$. For NMDA and GABA channels, *depr*=0. AMPA receptor desensitization, known to occur in the striatum (Akopian and Walsh, 2007; Carter et al., 2007), is simulated with a time dependent *depr* value. Each time an AMPA synapse is activated *depr* is incremented by 1.0, and the value of *depr* decays with a time constant of 100ms. NMDA receptors are modulated by the addition of a magnesium block object, where B=99 and A=18 (Equation 3).

(3)

$$\frac{A}{A + [Mg^{2+}] * exp(-Vm * B)}$$

Extracellular magnesium concentration is set to 1.4mM (Kerr and Plenz, 2002, 2004).These parameters closely match, but slightly accentuate the magnesium sensitivity seen in (Monyer et al., 1994). Excitatory inputs activate both an NMDA and an AMPA component with an NMDA/AMPA ratio of 2.75/1 (Ding et al., 2008), except in the 'no NMDA' condition where the NMDA channel was removed. The fraction of the NMDA receptor current carried by calcium was set to 10% (Wolf et al., 2005), and the AMPA receptors were not calcium permeable. A GHK object was employed to calculate the driving potential of the calcium current through the NMDA receptor independently of the driving potential of the total NMDA current. An empirically determined multiplicative factor of 35e-9 was needed convert the conductance output of the magnesium block object to the permeability required by the GHK object.

*Synaptic inputs and spike timing*. Upstates were generated using excitatory and inhibitory Poisson input trains of 300ms duration as input. Inhibitory input frequencies were set to 70Hz and these trains were completely independent of excitatory inputs. A variety of excitatory input patterns were simulated: A flat input of 40Hz and a series of graded inputs at different strengths (see figure 5 and appendix table 6). Unless otherwise specified, gradient 'G3' was used for the upstate simulations. APs were evoked at specific times within the upstate by a 5ms 800pA current injection into the soma. AP timing was measured from the beginning of the upstate to the beginning of the 5ms depolarization. The actual peak of the AP varied by <2ms, and our previous work has shown that spike variability on this scale does not affect calcium results (Evans et al., 2012). During the STDP protocols, one segment of dendrite 44um from the soma was given a single input at positive or negative Δt from the AP with no other synaptic inputs.

*Voltage clamp of calcium currents.* All animal handling and procedures were in accordance with the National Institutes of Health animal welfare guidelines and were approved by the George Mason University institutional animal care and use committee (IACUC). C57B6 male and female mice (Charles River, p13-21) were anesthetized with isoflurane and euthanized. Every effort was made to minimize anxiety and pain. Brains were extracted and cut 350µm thick using a vibratome (Leica VT 1000S) in ice cold sucrose slicing solution (in mM: KCL 2.8, Dextrose 10, $NaHCO_3$ 26.2, $NaH_2PO_4$ 1.25, $CaCl_2$ 0.5, $Mg_2SO_4$ 7, Sucrose 210). Slices were immediately placed in an incubation chamber containing artificial cerebrospinal fluid (aCSF) (in mM: NaCl 126, $NaH_2PO_4$ 1.25, KCl 2.8,$CaCl_2$, $Mg_2SO_4$ 1, $NaHCO_3$ 26.2, Dextrose 11) for 30 minutes at 33°C, then removed to room temperature (22-24°C) for at least 90 more minutes before use. Recording aCSF was modified by replacing $Mg_2SO_4$ with $Mg_2Cl$ and including either 2mM $Ca_2Cl$ or 2mM $Ba_2Cl$. TTX (0.5µM) and 4-AP (4mM) were added to block sodium and potassium channels respectively. Slices were individually placed in a submersion chamber (ALA scientific) and cells were visualized using differential interference contrast imaging (Zeiss Axioskop2 FS plus). Pipettes (3-5MΩ) were pulled from borosilicate glass on a laser pipette puller (Sutter P-2000), coated with candle wax (to reduce pipette capacitance), and fire-polished (Narishige MF-830). Pipettes were filled with a cesium based internal solution (in mM Cs-gluconate 85, Cs3-citrate

10, KCl 1, NaCl 10, HEPES 10, EGTA 1.1, $CaCl_2$ 0.1, $MgCl_2$ 0.25, TEA-Cl 15, Mg-ATP 3.56, Na-GTP 0.38) pH 7.26 (Rankovic et al., 2011). Voltage clamp recordings were obtained on the HEKA EPC-10 and sampled at 20KHz. Data were acquired in Patchmaster (HEKA Elektronik). Analogue 3-pole (10kHz) and 4-pole (2.9kHz) Bessel filters were applied. Series resistance (4-15MΩ) and capacitance were compensated.

*Simulation and analysis.* All simulations used a time step of 5 μs and were repeated using three random number seeds unless otherwise specified. Four dendrites from each simulation were averaged together to estimate the calcium for a single simulation. For the STDP simulation, calcium from the dendrite receiving only the single timed glutamatergic input was measured from each random number seed. The strength of the dependence of calcium on AP timing (the "calcium timing ratio") was evaluated by averaging the two latest AP conditions (175ms and 290ms) and normalizing them by the highest calcium elevation of that condition (usually 10, 20 or 30ms). For all these cases graphs report mean and standard deviation across the three random number seeds. Data shown in figures 3-5 are run for one random seed and the data are presented as mean±SEM across four measured dendritic segments. Statistical significance was evaluated using the SAS procedure GLM, and considered significant for $p<0.01$. In the case of multiple comparisons, a Bonferroni correction was applied. This model is available on ModelDB.

## Results

### *Part 1: Mechanisms underlying the calcium sensitivity to AP timing during the upstate.*

Here we validate our model against published data and describe two mechanisms that may account for the relationship between calcium and AP timing during cortico-striatal upstates. We confirm that both mechanisms make calcium elevation sensitive to AP timing, and test how these manipulations interact with distance from the soma and the presence of NMDA receptors.

*Intrinsic physiology and calcium dynamics in the MSN model match published data*

We developed a multi-channel, multi-compartmental biophysical model of a MSN, tuned to match electrophysiological characteristics of whole cell current clamp recordings in

slice (figures 1A&B and see methods), and upstate characteristics (figures 1C&D) such as fast depolarization into the upstate, 200-500 ms plateau, and slower repolarization back to the downstate. To accurately model the calcium dynamics in response to electrical activity, this model included a shell-based representation of calcium pools in order to simulate diffusion, calcium buffers (appendix table 4), and submembrane pumps. The intrinsic calcium activity of this MSN was tuned to match published data showing sodium channel-dependent back-propagation of APs into the proximal dendrites (Kerr and Plenz, 2002) (figure 2B) and strong AP decay in distal dendrites (Day et al., 2008) (figure 2C). Dendritic VGCC channel permeabilities were adjusted to qualitatively match their contribution to dendritic calcium elevations during single back-propagating APs (Carter and Sabatini, 2004) (figure 2D). Despite the maximal permeabilities being consistent throughout the distal dendrites (appendix table 3), the contribution of the T-type calcium channels increased with distance from the soma and the contributions of the L and R type calcium channels decreased (figure 2D). Though the contribution of the T-type calcium channel in our model at 44μm from the soma is not quite as strong as shown in Carter and Sabatini (2004), we consider these results to be a reasonably good match because Carter and Sabatini were sampling a range of distances from the soma. We used this tuned model for all subsequent upstate simulations without any further adjustment to the intrinsic calcium.

*Two mechanisms can account for the relationship between calcium and AP timing*

Calcium imaging studies have shown that APs evoked early in the upstate correspond to higher dendritic calcium elevations than APs evoked late in the upstate (Kerr and Plenz, 2004). We hypothesize that two main mechanisms could cause this relationship between calcium and AP timing. First, if the AP back propagated strongly when it occurred early in the upstate, but weakly when it occurred late in the upstate, the calcium peaks would also be strong early and weak late. Second, even if the AP back propagated with equal strength early and late in the upstate, the calcium response could desensitize during the upstate to show the same strong early, weak late calcium pattern. Because the dendritic voltage during upstates has not been recorded, it is not known if the AP back propagates differently early and late in the upstate.

Therefore we test both configurations in the computational model to see how well each matches published data.

We simulated the calcium in response to a range of AP times during an upstate for two model variations. Upstates are simulated in the model MSN using randomly generated Poisson trains of excitatory and inhibitory input. Using the same random seed to generate the pattern of input, the exact same subthreshold upstate could be repeated with several different AP timings. Each upstate was repeated with a somatic current injection evoking an AP delayed 10, 20, 30, 50, 100, 175, or 290 ms from upstate onset.

First, a slow inactivation component, which has been measured in striatal sodium channels (Ogata and Tatebayashi, 1990) was added to dendritic sodium channels (Migliore, 1996). This NaSI condition indeed caused the AP to back propagate more strongly early in the upstate than late (figure 3A, top panel), and the corresponding calcium elevations varied with AP timing during the upstate (figure 3A, bottom panel). Secondly, calcium dependent inactivation (CDI, see appendix table 2 for equation) of voltage gated calcium channels (VGCCs) (Liang et al., 2003) was added to L, N, and R type calcium channels in our model. When applied to the model, the CDI condition resulted in strong electrical back propagation of the AP both early and late in the upstate (figure 3B, top panel), but the calcium elevation still varied with AP timing (figure 3B, bottom panel). These two conditions, CDI and NaSI, resulted in APs that were indistinguishable at the soma in size and shape (figure 3C). If neither manipulation was applied, the relationship between calcium and AP timing was very weak (figure 3D), and if both were applied simultaneously, the results were not different from the NaSI condition alone (data not shown).

To confirm that high voltage activated (HVA) channels actually undergo CDI in the striatum, we voltage clamped HVA calcium currents (by holding at -40mV and stepping to +10mV) and repeated measurements using barium (which causes minimal CDI) and calcium (which causes strong CDI). The ratio of the decayed current (sampled after 180ms) to the peak current (sampled within first 50 ms) was taken as the CDI ratio. In all striatal cells recorded

(n=5), the CDI ratio was much stronger in calcium than in barium ($p<0.00001$, paired T-test) (figures 3E&F).

An additional mechanism could theoretically account for a decrease in calcium elevation late in the upstate. An *increase* in buffer capacity and/or pump capacity during the upstate could increase the rate of calcium removal and thus decrease the free calcium. Changes in buffer capacity due to protein synthesis are unlikely at the temporal scales being investigated. One report of a changes in pump capacity actually demonstrates an activity dependent *decrease* in the sodium calcium exchanger (Scheuss et al., 2006). Because an activity dependent decrease in pump activity would result in *more* calcium late in the upstates, this mechanism is unlikely to contribute to the decrease in calcium elevation observed late in the upstate(Kerr and Plenz, 2004). Furthermore, simulations which evaluate the effect of changing pump capacity reveal an insignificant effect on calcium timing ratio for both CDI and NaSI conditions (figure 4).

In addition to changes in pump capacity, we evaluated the robustness of our computational model to other parameter variations (figure 4). We systematically varied each parameter directly relating to calcium (buffers, pumps, NMDA calcium and each VGCC) by ±20% and compared the calcium relationship with AP timing for each condition to the controls. None of these manipulations significantly altered the relationship between calcium and AP timing in either CDI ($F(18, 75) = 0.15$, $p>0.9$) or NaSI ($F(18, 75) = 0.49$, $p>0.9$) (averaged over four dendrites for one random seed). These tests confirm that our main effect is robust to variation in calcium influx, buffering, and pump extrusion.

*The calcium-AP relationship depends on input shape and distance from the soma.*

The strength of the relationship between calcium elevation and AP timing is modulated by the shape of the cortical input creating the upstate. We simulated a range of input gradients, (figures 5A&B) and the strength of the calcium dependence on AP timing varied with the strength of the gradient (figures 5D&E). While both the NaSI and CDI conditions showed a dependence on input steepness, the effect was stronger for CDI (calcium timing ratio = 0.59±0.0008 G3, 0.35±0.01 flat; $p<0.0001$), than for NaSI (calcium timing ratio = 0.57±0.04 G3,

0.54±0.07 flat; p>0.9). This result leaves open the possibility that synaptic input pattern alone is sufficient for AP timing effects on calcium. To test this we repeated simulations using gradient G3 in a model with neither CDI nor NaSI. Without either of these mechanisms, the calcium dependence on AP timing was essentially absent (figure 3D). Therefore, while the input gradient *contributes* to the calcium dependence on AP timing, it is not sufficient to *generate* it. Because the simulations fit published data more accurately when the synaptic inputs were weighted toward the beginning of the upstate, we used gradient G3 as the upstate-generating input, unless otherwise specified.

Calcium imaging in organotypic co-cultures reveals that the calcium elevation due to the upstate and the relationship between calcium and AP timing increases with distance from the soma (Kerr and Plenz, 2004). To test whether both CDI and NaSI show this increase in the calcium AP timing relationship, the calcium signal is recorded at progressively more distal dendrites during upstate simulations (figure 6A). Both CDI and NaSI show an increase in the strength of the calcium dependence on AP timing (calcium timing ratio) between primary, secondary, and tertiary branches (figures 6B&C insets). Therefore, in this case, both conditions equally match the published data.

Because the organotypic co-culture study did not record the calcium signals of distal dendrites (Kerr and Plenz, 2004), and we have previously shown that the effect of the back-propagating AP on calcium influx is attenuated in distal dendrites (Evans et al., 2012), we tested the relationship between calcium and AP timing distally. Figure 6 shows that distally the relationship between calcium and AP timing *decreases* with distance from the soma. This result implies that there is an optimal distance from the soma where the timing of the AP has the strongest effect on the corresponding calcium signal. More proximal dendrites are larger and have lower impedance, causing a reduced effect of synaptic inputs, and more distal dendrites are subject to the decay of the back-propagating AP causing a weaker relationship between calcium and AP timing. The optimal distance in our model is the first tertiary dendritic segment, 44-62µm from the soma. Interestingly, it is exactly this distance from the soma that has been shown to have the highest density of dendritic spines (Berlanga et al., 2011).

*CDI replicates the effect of NMDA receptor blockade on the relationship between calcium and AP timing*

Previous work demonstrated that the relationship between calcium influx and AP timing is dependent on the activation of the NMDA receptors (Kerr and Plenz, 2004). Therefore, we tested whether our two mechanisms (CDI and NaSI) were each dependent on the NMDA receptor by running upstate simulations with and without the NMDA receptors. Simulations revealed that removing the NMDA receptors greatly reduced the strength of the relationship between AP timing and calcium influx for the CDI condition (calcium timing ratio = 0.59±0.0008 cntrl, 0.30±0.054 no NMDA; $p<0.0001$), but did not reduce it for the NaSI condition (figure 7). In the NaSI condition, calcium elevations corresponding to both the early and the late APs were reduced with NMDA blockade, resulting in essentially the same *relationship* between calcium peak and AP timing (calcium timing ratio = 0.57±0.04 cntrl, = 0.61±0.06 no NMDA; $p>0.9$; figure 7A inset). Because the CDI condition matches the dependence of this calcium timing ratio on NMDA receptors and the NaSI condition does not, our model predicts that CDI is more likely to be a mechanism controlling this relationship.

Because the input gradient strongly influences the relationship between calcium and AP timing (figure 5), we repeated the NMDA and no NMDA comparison for the flat input condition. In the CDI condition, removing NMDA receptors during flat inputs caused a decrease in the calcium timing ratio (0.35±0.01 flat, 0.22±0.03 flat no NMDA, $p<0.01$) (figure 7B), even though the effect of removing NMDA receptors was much stronger for the G3 input gradient (figure 7A). In the NaSI condition, neither the G3 gradient input nor the flat input resulted in NMDA dependence of the calcium timing ratio. In contrast to the flat CDI condition, the flat NaSI condition showed a surprising enhancing of the relationship between calcium and AP timing due to blocked NMDA receptors (calcium timing ratio = 0.54±0.07 flat, 0.74±0.03 flat no NMDA; $p<0.01$; figure 7B inset). This enhancement clearly does not replicate published data (Kerr and Plenz, 2004), further supporting CDI as an essential mechanism underlying the relationship between calcium and AP timing.

In conclusion, we find that the CDI model better fits the published data. Specifically, the relationship between calcium and AP timing is dependent on NMDA receptors only in the CDI case. Our voltage clamp experiments support this as a plausible mechanism because they show that CDI does indeed occur in the HVA calcium channels of the striatum. Therefore, all subsequent simulations are run using the CDI condition.

***Part 2: Effect of neuromodulation and implications for* in vivo *plasticity.***

Here we use the model to investigate several aspects of plasticity during cortico-striatal upstates. We test how intrinsic and synaptic excitability, which can balance each other in homeostatic plasticity, affect the relationship between calcium and AP timing, and investigate the mechanisms controlling calcium binding to downstream targets which can influence the direction of plasticity at a synapse. Finally, we test whether spike timing dependent plasticity (STDP) pairings are modulated by their timing within the upstate.

*Modulation of intrinsic, but not synaptic excitability alters calcium relationship with AP timing*

Differences in stimulation patterns or changes in neuromodulator availability can alter MSN intrinsic excitability, which in turn can affect plasticity. The intrinsic excitability of the dendrite depends on the composition of voltage gated potassium and sodium channels as well as the input resistance. Slice experiments have shown that dopamine depletion in the striatum increases intrinsic excitability of MSNs (Fino et al., 2007) and that this excitability increase is due to a two fold increase in the inactivation speed of A-type potassium currents (Kaf) (Azdad et al., 2009). Another potassium channel that can both modify dendritic excitability and be dynamically altered in response to neuromodulation is the inwardly rectifying potassium current (Kir). Acetylcholine M1 receptor activation causes a strong (40%) reduction of this current in one class of MSN (Shen et al., 2007).

To evaluate the effect of excitability on the sensitivity of calcium to AP timing, we repeated simulations with either inactivation of Kaf twice as fast as the control condition or the conductance of the inwardly rectifying Kir channel set to 60% of its control value. Our results show that faster Kaf inactivation makes the calcium elevation corresponding to the upstate

more sensitive to AP timing (figure 8A). Specifically this modification causes a calcium increase in response to APs early in the upstate, but no change in calcium elevation in response to APs late in the upstate (calcium timing ratio = 0.47±0.01 cntrl, = 0.57±0.01 fast Kaf inact; $p<0.005$). In contrast to the strong effect seen with Kaf modification, the change in Kir affects neither the absolute calcium nor the relationship between AP timing and calcium elevation (calcium timing ratio = 0.59±0.0008 cntrl, 0.58±0.0005 60% Kir; $p>0.9$) (figure 8C).

The increase in intrinsic excitability (via fast Kaf inactivation) may be a homeostatic mechanism deployed by the neuron to compensate for a decrease in synaptic excitability (via reduced AMPA receptor activity) that occurs with dopamine depletion (Azdad et al., 2009). The AMPA receptor plays a strong role in the local depolarization of the dendrite, and has been shown to influence the effect of back-propagating APs on NMDA calcium (Holbro et al., 2010). We therefore hypothesized that increased synaptic excitability implemented by removing AMPA receptor desensitization would reduce calcium sensitivity to AP timing. Surprisingly, when AMPA receptor desensitization was removed, the calcium dependence on AP timing was not altered (calcium timing ratio = 0.47±0.009 cntrl, 0.48±0.03 no AMPA desens; $p>0.9$) (Figure 8B). These results show that increases in synaptic excitability and increases in intrinsic excitability do not affect calcium during the upstate in the same way. This also suggests that a change in intrinsic excitability cannot fully compensate for a change in synaptic excitability with regards to calcium sensitivity to AP timing and therefore has implications for upstates during dopamine depletion pathologies such as Parkinson's Disease.

*Fast and slow calcium binding partners are differentially influenced by AP timing and AP number.*

Since calcium is required for plasticity in the striatum (Fino et al., 2010), it has been suggested that the calcium elevations during upstates could cause potentiation or depression (Kerr and Plenz, 2004). However the factors that determine whether calcium causes potentiation or depression are still not clear. Recent studies suggest that the dynamics of calcium influx control preferential binding of calcium to disparate targets (Goldberg et al., 2009; Kubota and Waxham, 2010). To test whether the timing of the AP within the upstate would

influence not only calcium elevation, but also the binding partners which calcium preferred, we made use of our calmodulin buffer which has a fast binding N site (CaMN) and a slow binding C site (CaMC).

During the upstate simulations, the peak concentration of bound CaMN is more strongly affected by the timing of the AP within the upstate than the peak concentration of bound CaMC (figure 9A). The slower binding and unbinding of calcium from the CaMC site smoothes the effect of the AP, making its timing irrelevant, while the fast binding and unbinding of the CaMN site makes it sensitive to AP timing. Figure 9 shows the peak bound CaMC (9A) and CaMN (9B) sites as a function of AP timing within the upstate (black symbols).While the peak bound CaMC is always higher than the peak bound CaMN (due to the higher affinity of calcium for the C site than the N site), it is clear that binding to the CaMN site is sensitive to AP timing, but binding to the CaMC site is not.

Another way that information can be conveyed during the upstate is through number of APs, rather than the specific timing of a single AP. To test whether the N and C sites of calmodulin were differentially sensitive to AP number, we ran upstate simulations with 1 to 11 APs. To prevent AP timing from influencing the bound buffer elevation, the timing of the initial AP was kept constant (20ms from upstate onset), and each AP was added 20ms after the most recent one (for a frequency of 50Hz). In contrast to the AP timing condition, the peak bound CaMC site increased with the total number of APs, while the peak bound CaMN remained constant (figure 9, gray symbols). These results demonstrate that the two lobes of calmodulin are differentially sensitive to either the precise timing of the AP (CaMN) or the total number of APs (CaMC) within the upstate. Because the bound N and bound C sites differentially influence CaM's ability to bind to CaM dependent kinase type 2 (CaMKII), a molecule implicated in synaptic strengthening (Forest et al., 2008), the specific combination of AP timing and AP number during the upstate may determine whether a given synapse will undergo potentiation or depression.

*AP timing during the upstate interacts with spike timing dependent plasticity protocols*

When APs are paired with precisely timed glutamatergic inputs, a cortico-striatal synapse can undergo spike timing dependent plasticity (STDP) (Fino et al., 2010). However *in vivo* neurons are subject to barrages of synaptic inputs during the upstate; thus a crucial question is whether spike timing influences calcium under *in vivo* like conditions. We have previously shown that the NMDA mediated calcium during STDP protocols correlates with synaptic potentiation (Evans et al., 2012). Here we use similar measurements to test how specifically timed pairings during the upstate would affect NMDA mediated calcium.

Because the spatial constraints of dendritic spines could alter the calcium dynamics, we added a single spine with an NMDA calcium pool to the first tertiary dendritic segment. In order to precisely control the timing of the pre and post-synaptic stimulations, we reserved a single tertiary dendritic segment, 44µm from the soma, and stimulated its spine only one time during the entire upstate. The time of this stimulation was varied (Δt) around an early (20ms after onset) upstate AP and a late (175ms after onset) upstate AP (figure 10, inset). The NMDA mediated calcium was recorded for each interval through a separate NMDA calcium pool (Evans et al., 2012). Pairing synaptic input with the AP showed a distinctive STDP-curve both early and late in the upstate (figure 10). As in our previous model (Evans et al., 2012), the positive intervals showed higher NMDA mediated calcium peaks.

The upstate depolarizes the dendrite even without an AP and subthreshold depolarizations have been shown to cause synaptic plasticity in MSNs (Fino et al., 2009). Thus, it is possible that the timing of the synaptic input relative to the subthreshold upstate could produce an STDP-like curve even without an AP. To demonstrate that the timing of the AP is indeed contributing to the shape of the STDP curve, we ran simulations in the absence of an AP (figure 10, open symbols). The stimulations given late in the upstate have no temporal sensitivity without the AP, while the stimulations early in the upstate demonstrate moderate temporal sensitivity even without the AP. In both the early and late AP cases, however, the AP 'sharpens' the curve, lowering the NMDA calcium during negative intervals and increasing NMDA calcium during positive intervals relative to the no AP condition. This 'sharpening' effect is much stronger when the stimulated synapse is on the spine than on the dendritic shaft (data

not shown), suggesting that indeed the spatial constraints of the spine head influence the relationship between calcium and the backpropagating AP.

These results suggest that specific pre and post-synaptic pairings could undergo STDP even during an upstate. Because the NMDA mediated calcium is higher early in the upstate than later in the upstate, our model predicts that pairings occurring early in the upstate will have a slight bias toward potentiation when compared to pairings occurring late in the upstate.

## Discussion

Upstates in the striatum drive large dendritic calcium transients which may control naturally occurring potentiation and depression of MSN synapses during sleep. The distinct up and downstate pattern is a trademark of the anesthetized or sleeping striatum and is much weaker during wakefulness (Mahon et al., 2006). We have implemented highly realistic calcium dynamics in a biophysical model of a MSN to study the factors governing these calcium elevations during upstates and to investigate the implications of a timing dependent calcium elevation on synaptic plasticity.

### *Is CDI or NaSI more likely?*

We first evaluated two mechanisms that cause the strong relationship between calcium elevation and AP timing within the upstate: NaSI and CDI. Both mechanisms matched the published data regarding the dependence of calcium on AP timing and the effects of distance from the soma on calcium elevation, but they did not both match other published effects such as NMDA dependence. Because CDI matched the published NMDA dependence of the timing dependent calcium elevations while NaSI did not, our model predicts that CDI is more likely the mechanism producing the effect of AP timing.

It is important to note that these are not the only possible mechanisms that could account for a calcium relationship with AP timing. Pump extrusion, for example, could be altered over the course of the upstate or dependent on number or frequency of action potentials (Scheuss et al., 2006). Further experiments are needed to confirm that CDI is the main mechanism for the calcium relationship with AP timing.

*Three testable predictions*

First, the simulations fit published data more accurately when the synaptic inputs are weighted toward the beginning of the upstate (figure 5). Thus, our model predicts that the cortico-striatal upstates are initiated by strong glutamatergic inputs from the cortex. Electrophysiological recordings from organotypic triple co-cultures (Kerr and Plenz, 2004) and *in vivo* (Schulz et al., 2009) demonstrate variability in upstate shape. However, the upstates often show steep rise times at initiation rather than slow increases (figures 1C&D). In addition, recent experimental work has shown that striatal upstates can be sustained hundreds of milliseconds after the glutamatergic barrage has ended (Flores-Barrera et al., 2009; Plotkin et al., 2011) (but see also Kasanetz et al., 2006), indicating that it is indeed possible that naturally occurring upstates could have strong initial inputs that decrease or even disappear over the duration of the upstate. While one study found that distal inputs were able to induce upstates more strongly than proximal (Plotkin et al., 2011), the excitatory and inhibitory inputs in our model are distributed equally throughout the cell and differences based on spatial distribution of inputs were not explored. Experiments using calcium hotspot imaging (Varga et al., 2011) in organotypic co-cultures could test our model prediction that glutamatergic inputs during the upstate are weighted toward upstate onset. In addition this technique could be used to test the spatial distribution of synaptic inputs during spontaneous upstates.

Second, simulations demonstrate that there is a specific distance from the soma which shows optimal sensitivity to AP timing. In our model it is the first segment of the tertiary dendrite, 44-62μm from the soma. However because each neuron is slightly different, it is likely that the size and location of this optimal distance could be variable. Therefore our simulations predict that for a given neuron there will be an optimal distance that displays a very strong relationship between calcium and AP timing, though it will not necessarily be the exact same distance for every neuron. Synapse and spine counting studies have shown that excitatory synapse density and spine density is highest between 30-60μm from the soma, declining sharply in the proximal direction, and declining more gradually in the distal direction (Berlanga et al., 2011). It is possible that optimal sensitivity to AP timing at this location increases calcium-

based plasticity and consequently spine growth and excitatory synapse development. While the changes in sensitivity to AP timing proximal to the soma have already been shown (Kerr and Plenz, 2004), experiments imaging calcium on very distal dendrites during striatal upstates could test our model prediction that the sensitivity to AP timing decreases in the distal dendrites.

Third, simulations reveal a means through which MSNs can dynamically alter their sensitivity to AP timing during the upstate by modulating their intrinsic excitability. Increasing the speed of Kaf inactivation accentuated calcium's dependence on AP timing during the upstate. This doubling of the Kaf inactivation kinetics occurs in the striatum in response to dopamine depletion (Azdad et al., 2009). Azdad et al.(2009) suggest that this excitability change is a form of homeostatic plasticity, increasing *intrinsic* excitability to compensate for a loss in *synaptic* excitability. However, as we have shown, this specific intrinsic excitability change increases the calcium dependence on AP timing, while a synaptic excitability change (the removal of AMPA receptor desensitization) does not alter the relationship. Thus, the balance is not necessarily restored accurately. Such a compensation would result in an increased sensitivity to AP timing which may be too strong for optimal function. Indeed, a change in calcium dependence on AP timing could result in plasticity imbalances and consequently contribute to symptoms of dopamine depletion pathologies such as Parkinson's Disease. Because we did not see an effect of Kir modification, our simulations show that not all changes in potassium-based intrinsic excitability will result in altered calcium dynamics. While we did not model all the effects of dopamine depletion, our model predicts that alterations in Kaf observed during dopamine depletion will increase the dependence of calcium on AP timing. This prediction could be experimentally tested by pharmacologically or genetically manipulating the Kaf channel in organotypic co-cultures to test how changes in kinetics affected the calcium elevation during the upstate. Similarly, application of cyclothiazide to inhibit AMPA desensitization under the same conditions could reveal whether this aspect of synaptic excitability affects the calcium elevation during the upstate.

*Implications for plasticity*

Calcium elevation is necessary for both the potentiation and depression of cortico-striatal synapses (Fino et al., 2007). How calcium can cause these opposing effects is still a question up for debate. Several mechanisms have been postulated, for example, that the total amount of calcium determines the direction of plasticity (Graupner and Brunel, 2012), that the channel allowing calcium influx determines plasticity (Fino et al., 2010), or that the binding of calcium to downstream targets makes the difference (Lisman, 1989).

It is clear from our results that *if* the total amount of calcium determines the direction of plasticity (high calcium=potentiation; low calcium=depression), upstates that contain early APs will be more likely to potentiate synapses than upstates containing late APs. However, it is not clear that the *amount* of calcium is the only important factor. Therefore, we investigated differences in calcium binding during early and late APs. We found that the fast binding of the CaMN site was sensitive to AP timing, but the slow binding of the CaMC site was not. Previous studies have shown that fast binding partners are more sensitive to the backpropagation of a single AP than slow binding partners (Markram et al., 1998). Our work supports this idea and extends it to an *in vivo*-like context within the upstate. Importantly, we demonstrate that there is a dichotomy in the way that each calmodulin binding site responds to different types of information carried by the upstate. Specifically, the CaMN site is sensitive to AP timing, while the CaMC site is sensitive to AP number. These simulations reveal differential functions of calmodulin lobes without the spatial scale implemented in single spine simulations (Kubota and Waxham, 2010). Calcium binding to the CaMN site alone is able to partially activate CaMKII, a molecule strongly implicated in synaptic strengthening (Forest et al., 2008). The CaMN site's preferential response to APs early in the upstate implies that the APs early in the upstate will more efficiently trigger mechanisms for increasing synaptic strength.

In addition, our results can be extended to other calcium binding partners. Our model predicts that in general fast binding partners will be sensitive to AP timing, while slow binding partners will be sensitive to AP number. This result, in combination with future research revealing the kinetics of plasticity-related calcium binding partners, will shed light on which plasticity mechanisms are sensitive to specific upstate characteristics.

STDP pairings show robust synaptic plasticity in cortico-striatal brain slice and our previous work (Evans et al., 2012) demonstrates that the simulated NMDA calcium under these conditions is an excellent predictor of synaptic potentiation. Here we show that during noisy *in vivo* like conditions, STDP curves can still be established for independent dendritic and spine compartments. This finding suggests that STDP can occur during sleep, when the upstate-downstate pattern is most prominent (Mahon et al., 2006). Plasticity under these conditions may play a role in memory consolidation mediated by replay of cortical activity during sleep (Ribeiro et al., 2004; Lansink et al., 2009)

Our simulations compliment the experimental findings of Fino et al., (2009), which show that subthreshold depolarizations paired with pre-synaptic stimulation can induce synaptic plasticity in MSNs. They show that the curves elicited by pairing pre-synaptic stimulation with subthreshold post-synaptic depolarization are wider and less 'directional' than those elicited by pairing pre-synaptic stimulations with suprathershold stimulations containing APs. Similarly, our simulations show that the timing intervals which evoke elevated calcium under the subthreshold (no AP) condition early in the upstate are wider and shallower than the same stimulations paired with an AP.

It has been hypothesized that one population of synapses controls the upstate, but that a separate set of inputs drives the AP (O'Donnell and Grace, 1995; Kasanetz et al., 2006). If this is indeed the case, a specific STDP-like pairing could easily occur on a dendritic segment or spine during the upstate. If an input consistently drives an AP during the upstate, it would consistently show a positive $\Delta t$ and be potentiated. If an input simply drives the upstate, but not the AP, it would be equally likely to fall in a positive or negative $\Delta t$ relative to the AP and would not be consistently potentiated. In this way the STDP control of calcium influx could control the direction of plasticity for specific synapses despite the calcium influx due to the upstate as a whole. On the other hand, the STDP control of calcium influx is not completely independent of timing during the upstate. We found that the whole STDP curve is shifted slightly upwards, towards higher NMDA calcium, when the AP is early in the upstate compared to when the AP is late. This suggests that even if the plasticity of a synapse is based solely on

602 STDP principles, the pairings that occur early in the upstate will be slightly biased toward
603 potentiation.

604 *Conclusion*

605 Our model is the most advanced biophysical MSN model to date and is a useful tool for
606 studying the calcium dynamics in the striatum. We have used it to investigate the mechanisms
607 which underlie the non-linear calcium dynamics corresponding to AP timing during striatal
608 upstates, and it could easily be extended to answer other essential questions about striatal
609 function and plasticity.

## References


**Akopian G, Walsh JP**. Reliable long-lasting depression interacts with variable short-term facilitation to determine corticostriatal paired-pulse plasticity in young rats. *J. Physiol. (Lond.)* 580: 225–240, 2007.

**Allbritton NL, Meyer T, Stryer L**. Range of messenger action of calcium ion and inositol 1,4,5-trisphosphate. *Science* 258: 1812–1815, 1992.

**Azdad K, Chàvez M, Don Bischop P, Wetzelaer P, Marescau B, De Deyn PP, Gall D, Schiffmann SN**. Homeostatic plasticity of striatal neurons intrinsic excitability following dopamine depletion. *PLoS ONE* 4: e6908, 2009.

**Bargas J, Howe A, Eberwine J, Cao Y, Surmeier DJ**. Cellular and molecular characterization of Ca2+ currents in acutely isolated, adult rat neostriatal neurons. *J. Neurosci.* 14: 6667–6686, 1994.

**Berlanga ML, Price DL, Phung BS, Giuly R, Terada M, Yamada N, Cyr M, Caron MG, Laakso A, Martone ME, Ellisman MH**. Multiscale imaging characterization of dopamine transporter knockout mice reveals regional alterations in spine density of medium spiny neurons. *Brain Res.* 1390: 41–49, 2011.

**Brevi S, de Curtis M, Magistretti J**. Pharmacological and biophysical characterization of voltage-gated calcium currents in the endopiriform nucleus of the guinea pig. *J. Neurophysiol.* 85: 2076–2087, 2001.

**Carter AG, Sabatini BL**. State-dependent calcium signaling in dendritic spines of striatal medium spiny neurons. *Neuron* 44: 483–493, 2004.

**Carter AG, Soler-Llavina GJ, Sabatini BL**. Timing and location of synaptic inputs determine modes of subthreshold integration in striatal medium spiny neurons. *J. Neurosci.* 27: 8967–8977, 2007.

**Day M, Wokosin D, Plotkin JL, Tian X, Surmeier DJ**. Differential excitability and modulation of striatal medium spiny neuron dendrites. *J. Neurosci* 28: 11603–11614, 2008.

**Ding J, Peterson JD, Surmeier DJ**. Corticostriatal and thalamostriatal synapses have distinctive properties. *J. Neurosci* 28: 6483–6492, 2008.

**Evans RC, Morera-Herreras T, Cui Y, Du K, Sheehan T, Kotaleski JH, Venance L, Blackwell KT**. The Effects of NMDA Subunit Composition on Calcium Influx and Spike Timing-Dependent Plasticity in Striatal Medium Spiny Neurons. *PLoS Comput. Biol.* 8: e1002493, 2012.

**Fino E, Deniau J-M, Venance L**. Brief subthreshold events can act as Hebbian signals for long-term plasticity. *PLoS ONE* 4: e6557, 2009.

**Fino E, Glowinski J, Venance L**. Bidirectional activity-dependent plasticity at corticostriatal synapses. *J. Neurosci* 25: 11279–11287, 2005.

**Fino E, Glowinski J, Venance L**. Effects of acute dopamine depletion on the electrophysiological properties of striatal neurons. *Neurosci. Res.* 58: 305–316, 2007.

**Fino E, Paille V, Cui Y, Morera-Herreras T, Deniau J-M, Venance L**. Distinct coincidence detectors govern the corticostriatal spike timing-dependent plasticity. *J. Physiol. (Lond.)* 588: 3045–3062, 2010.

**Flores-Barrera E, Laville A, Plata V, Tapia D, Bargas J, Galarraga E**. Inhibitory contribution to suprathreshold corticostriatal responses: an experimental and modeling study. *Cell. Mol. Neurobiol.* 29: 719–731, 2009.

**Foehring RC, Mermelstein PG, Song WJ, Ulrich S, Surmeier DJ**. Unique properties of R-type calcium currents in neocortical and neostriatal neurons. *J. Neurophysiol.* 84: 2225–2236, 2000.

**Forest A, Swulius MT, Tse JKY, Bradshaw JM, Gaertner T, Waxham MN**. Role of the N- and C-lobes of calmodulin in the activation of Ca(2+)/calmodulin-dependent protein kinase II. *Biochemistry* 47: 10587–10599, 2008.

**Goldberg JA, Teagarden MA, Foehring RC, Wilson CJ**. Nonequilibrium calcium dynamics regulate the autonomous firing pattern of rat striatal cholinergic interneurons. *J. Neurosci.* 29: 8396–8407, 2009.

**Graupner M, Brunel N**. Calcium-based plasticity model explains sensitivity of synaptic changes to spike pattern, rate, and dendritic location. *Proceedings of the National Academy of Sciences of the United States of America* (February 22, 2012). doi: 10.1073/pnas.1109359109.

**Halavi M, Polavaram S, Donohue DE, Hamilton G, Hoyt J, Smith KP, Ascoli GA**. NeuroMorpho.Org implementation of digital neuroscience: dense coverage and integration with the NIF. *Neuroinformatics* 6: 241–252, 2008.

**Holbro N, Grunditz A, Wiegert JS, Oertner TG**. AMPA receptors gate spine Ca(2+) transients and spike-timing-dependent potentiation. *Proc. Natl. Acad. Sci. U.S.A.* 107: 15975–15980, 2010.

**Kasai H, Neher E**. Dihydropyridine-sensitive and omega-conotoxin-sensitive calcium channels in a mammalian neuroblastoma-glioma cell line. *J. Physiol. (Lond.)* 448: 161–188, 1992.

**Kasanetz F, Riquelme LA, O'Donnell P, Murer MG**. Turning off cortical ensembles stops striatal Up states and elicits phase perturbations in cortical and striatal slow oscillations in rat in vivo. *J. Physiol. (Lond.)* 577: 97–113, 2006.

**Kerr JND, Plenz D**. Dendritic calcium encodes striatal neuron output during up-states. *J. Neurosci.* 22: 1499–1512, 2002.

**Kerr JND, Plenz D**. Action potential timing determines dendritic calcium during striatal up-states. *J. Neurosci* 24: 877–885, 2004.

**Kim M, Huang T, Abel T, Blackwell KT**. Temporal sensitivity of protein kinase a activation in late-phase long term potentiation. *PLoS Comput. Biol.* 6: e1000691, 2010.

**Kubota Y, Waxham MN**. Lobe specific Ca2+-calmodulin nano-domain in neuronal spines: a single molecule level analysis. *PLoS Comput. Biol.* 6: e1000987, 2010.

**Lansink CS, Goltstein PM, Lankelma JV, McNaughton BL, Pennartz CMA**. Hippocampus leads ventral striatum in replay of place-reward information. *PLoS Biol.* 7: e1000173, 2009.

**Liang H, DeMaria CD, Erickson MG, Mori MX, Alseikhan BA, Yue DT**. Unified mechanisms of Ca2+ regulation across the Ca2+ channel family. *Neuron* 39: 951–960, 2003.

**Lisman J**. A mechanism for the Hebb and the anti-Hebb processes underlying learning and memory. *Proc. Natl. Acad. Sci. U.S.A.* 86: 9574–9578, 1989.

**Mahon S, Vautrelle N, Pezard L, Slaght SJ, Deniau J-M, Chouvet G, Charpier S**. Distinct patterns of striatal medium spiny neuron activity during the natural sleep-wake cycle. *J. Neurosci.* 26: 12587–12595, 2006.

**Markram H, Roth A, Helmchen F**. Competitive calcium binding: implications for dendritic calcium signaling. *J Comput Neurosci* 5: 331–348, 1998.

**McNaughton NC, Randall AD**. Electrophysiological properties of the human N-type Ca2+ channel: I. Channel gating in Ca2+, Ba2+ and Sr2+ containing solutions. *Neuropharmacology* 36: 895–915, 1997.

**McRory JE, Santi CM, Hamming KS, Mezeyova J, Sutton KG, Baillie DL, Stea A, Snutch TP**. Molecular and functional characterization of a family of rat brain T-type calcium channels. *J. Biol. Chem.* 276: 3999–4011, 2001.

**Migliore M**. Modeling the attenuation and failure of action potentials in the dendrites of hippocampal neurons. *Biophys. J.* 71: 2394–2403, 1996.

**Monyer H, Burnashev N, Laurie DJ, Sakmann B, Seeburg PH**. Developmental and regional expression in the rat brain and functional properties of four NMDA receptors. *Neuron* 12: 529–540, 1994.

**Nisenbaum ES, Wilson CJ**. Potassium currents responsible for inward and outward rectification in rat neostriatal spiny projection neurons. *J. Neurosci* 15: 4449–4463, 1995.

**O'Donnell P, Grace AA**. Synaptic interactions among excitatory afferents to nucleus accumbens neurons: hippocampal gating of prefrontal cortical input. *J. Neurosci.* 15: 3622–3639, 1995.

**Ogata N, Tatebayashi H**. Sodium current kinetics in freshly isolated neostriatal neurones of the adult guinea pig. *Pflugers Arch* 416: 594–603, 1990.

**Oliveira RF, Kim M, Blackwell KT**. Subcellular location of PKA controls striatal plasticity: stochastic simulations in spiny dendrites. *PLoS Comput. Biol.* 8: e1002383, 2012.

**Pawlak V, Kerr JND**. Dopamine receptor activation is required for corticostriatal spike-timing-dependent plasticity. *J. Neurosci* 28: 2435–2446, 2008.

**Plotkin JL, Day M, Surmeier DJ**. Synaptically driven state transitions in distal dendrites of striatal spiny neurons. *Nat. Neurosci* 14: 881–888, 2011.

**Rankovic V, Landgraf P, Kanyshkova T, Ehling P, Meuth SG, Kreutz MR, Budde T, Munsch T**. Modulation of calcium-dependent inactivation of L-type Ca2+ channels via β-adrenergic signaling in thalamocortical relay neurons. *PLoS ONE* 6: e27474, 2011.

**Ribeiro S, Gervasoni D, Soares ES, Zhou Y, Lin S-C, Pantoja J, Lavine M, Nicolelis MAL**. Long-lasting novelty-induced neuronal reverberation during slow-wave sleep in multiple forebrain areas. *PLoS Biol.* 2: E24, 2004.

**Scheuss V, Yasuda R, Sobczyk A, Svoboda K**. Nonlinear [Ca2+] signaling in dendrites and spines caused by activity-dependent depression of Ca2+ extrusion. *J. Neurosci.* 26: 8183–8194, 2006.

**Schulz JM, Redgrave P, Mehring C, Aertsen A, Clements KM, Wickens JR, Reynolds JNJ**. Short-latency activation of striatal spiny neurons via subcortical visual pathways. *J. Neurosci.* 29: 6336–6347, 2009.

**Shen W, Hernandez-Lopez S, Tkatch T, Held JE, Surmeier DJ**. Kv1.2-containing K+ channels regulate subthreshold excitability of striatal medium spiny neurons. *J. Neurophysiol* 91: 1337–1349, 2004.

**Shen W, Tian X, Day M, Ulrich S, Tkatch T, Nathanson NM, Surmeier DJ**. Cholinergic modulation of Kir2 channels selectively elevates dendritic excitability in striatopallidal neurons. *Nat. Neurosci.* 10: 1458–1466, 2007.

**Steephen JE, Manchanda R**. Differences in biophysical properties of nucleus accumbens medium spiny neurons emerging from inactivation of inward rectifying potassium currents. *J Comput Neurosci* 27: 453–470, 2009.

**Stoetzner CR, Pettibone JR, Berke JD**. State-dependent plasticity of the corticostriatal pathway. *Neuroscience* 165: 1013–1018, 2010.

**Tkatch T, Baranauskas G, Surmeier DJ**. Kv4.2 mRNA abundance and A-type K(+) current amplitude are linearly related in basal ganglia and basal forebrain neurons. *J. Neurosci* 20: 579–588, 2000.

**Tuckwell HC**. Quantitative aspects of L-type Ca2+ currents. *Prog. Neurobiol.* 96: 1–31, 2012.

**Varga Z, Jia H, Sakmann B, Konnerth A**. Dendritic coding of multiple sensory inputs in single cortical neurons in vivo. *Proc. Natl. Acad. Sci. U.S.A.* 108: 15420–15425, 2011.

**Wilson CJ, Groves PM**. Spontaneous firing patterns of identified spiny neurons in the rat neostriatum. *Brain Res.* 220: 67–80, 1981.

**Wolf JA, Moyer JT, Lazarewicz MT, Contreras D, Benoit-Marand M, O'Donnell P, Finkel LH**. NMDA/AMPA ratio impacts state transitions and entrainment to oscillations in a computational model of the nucleus accumbens medium spiny projection neuron. *J. Neurosci* 25: 9080–9095, 2005.

**Yin HH, Mulcare SP, Hilário MRF, Clouse E, Holloway T, Davis MI, Hansson AC, Lovinger DM, Costa RM**. Dynamic reorganization of striatal circuits during the acquisition and consolidation of a skill. *Nat. Neurosci* 12: 333–341, 2009.

## Figure Captions:

**Figure 1.Computational model comparison with electrophysiological data. A**. Morphology of model MSN, not to scale. Soma is 16µm in diameter, primary dendrites are 12µm long, secondary dendrites are 14µm long, and tertiary dendrites are divided into 11 continuous 18µm long segments. **B**. Experimental and model voltage responses to somatic current injection of 260pA. Both demonstrate long latency to first action potential. Scale bars vertical: 10mV. horizontal: 100ms **C.** Experimental and model voltage traces showing synaptically evoked upstates. Scale bars vertical: 10mV. horizontal: 100ms. Experimental upstate is a spontaneous upstate recorded from organotypic triple co-culture (Blackwell and Plenz, *unpublished*). **D.** *In vivo* upstate traces show variability in upstate shape. Scale bars vertical: 5mV horizontal: 1s. Used with permission from John Reynolds.

**Figure 2: Intrinsic calcium signaling in the model matches published data**. **A.** Schematic drawing of dendritic segment showing diffusion of calcium between shells, extrusion of calcium via pumps, and influx of calcium via VGCCs. **B.** Model calcium signal (normalized to the signal seen at the soma) strongly responds to a single back propagating AP in proximal dendrites. When sodium channels are removed from the dendrites (TTX dend), calcium decreases with distance from the soma (Similar to Kerr and Plenz 2002 figure 7G). **C.** Model calcium signal (normalized to tertiary dendrite segment 1, 42µm from soma, in distal dendrites does not strongly respond to backpropagating AP (Similar to D1 neurons in Day et al. 2008 figure 1D). **D.** The contribution of VGCCs changes with distance from the soma even when the conductances are the same. The relative contribution of R and L type calcium channels is reduced in distal dendrites, while the relative contribution of T type calcium channels is increased (Contributions tuned to be qualitatively similar to Carter and Sabatini 2004 figure 2).

**Figure 3: Two basic mechanisms can account for the relationship between calcium elevation and AP timing during the upstate: reduced AP backpropagatation (NaSI) or reduced calcium response (CDI). A.** Reducing the back propagation of the APs through the implementation of NaSI causes a timing dependent reduction in the tertiary dendrite depolarization (top panel) and calcium response (bottom panel). **B.** Reducing the calcium response to depolarization through the implementation of CDI does not cause a reduction in the depolarization of the tertiary dendrite (top panel), but does cause a timing dependent reduction of the calcium response (bottom panel). **C.** APs were elicited at specific times by short (5ms) somatic depolarizations during the synaptically-induced upstate. There was very little difference in the shape of the upstate between the NaSI mechanism (gray) and the CDI mechanism (black). Scale bars vertical: 20mV horizontal: 50ms **D.** Average over 4 tertiary dendrites as a function of AP timing. **E.** Example traces showing CDI in high voltage activated calcium currents from a voltage clamped striatal neuron. Scale bars are vertical: 100pA. horizontal 50ms. **F.** Summary averaged CDI ratio (degree of reduction by end of 200ms) for all cells (n=5). *= $p<0.00001$, paired T-test.

**Figure 4: Robustness tests.** Changes in calcium parameters ±20% does not significantly change the main effect of AP timing dependent calcium concentration for either the NaSI condition (top) or the CDI condition (bottom). MM=Michaelis Menten pump (Kcat), CaM= calmodulin (both N and C site), cb=calbindin, NMDACa=fraction of calcium through NMDA receptor, L13=L-type calcium channel Cav1.3, L12=L-type calcium channel Cav1.2, N=N-type calcium channel, R=R type calcium channel, T=T-type calcium channel. All error bars ±SEM. Solid black line is mean for control condition and dotted black lines are ±SEM for control condition.

**Figure 5: Input pattern affects calcium dependence on AP timing**. **A.** Sub-threshold upstates of varying gradient patterns as measured at the soma. **B.** Schematic of input patterns (not to scale, see appendix table 6) **C.** Example traces of calcium in tertiary dendrites during each input pattern (no AP). **D.** Average of 4 tertiary dendrites as a function of AP timing for each input pattern. **E.** Calcium timing ratio for each input pattern, averaged over 4 tertiary dendrites for one random seed. All error bars ±SEM.

**Figure 6. Distance from soma affects calcium dependence on AP timing**. **A**. Morphology (not to scale) of one dendritic branch color-coded dark to light for increasing distance from soma. Example calcium traces for each dendritic segment, primary (P), secondary (S), tertiary1 (T1), tertiary2 (T2), and tertiary3 (T3) for both NaSI and CDI. Scale bars are vertical: 0.1 μM. horizontal: 100ms. **B**. Calcium dependence on AP timing for NaSI condition is most prominent at the proximal tertiary dendritic segment (T1). Inset: bar graph showing the calcium timing ratio between the calcium peak for early (highest point) and late (average of two last points) APs for each dendritic segment. All error bars are ± SD. **C.** Same as B, but for CDI condition.

**Figure 7. Dependence on NMDA receptors during flat and graded inputs. A.** Graded inputs result in a strong relationship between calcium signal and AP timing during the upstate. The calcium dependence on AP timing is reduced when the NMDA receptor is blocked only in the CDI condition. Note that the peak calcium elevations, but not the *relationship* between calcium and AP timing (calcium timing ratio, inset), are changed in the NaSI condition. Inset: bar graph showing the calcium timing ratio. All error bars are ± SD. (*=$p<0.0001$) **B.** When the upstate is elicited by flat input trains, the dependence of calcium peak on AP timing is reduced and the phenomenon is more weakly dependent on NMDA. Again this NMDA-dependence is observed for CDI, but not NaSI. Inset same as A.

**Figure 8. A change in intrinsic excitability alters calcium relationship with AP timing. A.** Fast Kaf inactivation (green traces) caused an increase in the strength of the calcium relationship with AP timing (*=p<0.005). Synaptic input with gradient G1 (see figure 5) was used to generate upstates to avoid spontaneous APs due to increased excitability. **B.** Removing AMPA receptor desensitization (blue traces) did not affect the calcium relationship with AP timing. Gradient G1 was used to generate upstates. **C.** Reducing Kir by 40% (red traces) did not affect the calcium relationship with AP timing.

**Figure 9. Preference for calcium binding partners differs with AP timing and AP number. A.** Peak bound calmodulin C site (CaMC) is sensitive to AP number (gray) but not AP time (black). **B.** Peak bound calmodulin N site (CaMN) is sensitive to AP time (black), but not AP number (gray). All error bars are ± SEM.

**Figure 10. STDP can occur during an upstate.** NMDA receptor mediated calcium in the spine head shows an STDP curve shape early and late in the upstate (filled squares), which requires the AP. Cntrl = NMDA stimulation alone. Inset: schematic of early and late AP with stimulation times (not to scale) during the upstate. Vertical lines represent timing of AP; dots represent timing of pre-synaptic stimulation.

# Appendix

| Channel Name | mh form | Steady State | tau | α or β equation | Vhalf (mV) | Slope (mV) | Rate |
|---|---|---|---|---|---|---|---|
| **Naf** | $m^3$ | sigmoid | *see table 2* | - | -25 | -10 | 1 |
| | h | sigmoid | *see table 2* | - | -60 | 6 | 1 |
| **Kir** | m | α/(α+β) | $(1e^{-3}/(\alpha+\beta))*2$ | α (exp) | - | -11 | 1e-5 |
| | | | | β (sigmoid) | 30 | -50 | 1.2 |
| **Kaf** | $m^2$ | α/(α+β) | $1e^{-3}/(\alpha+\beta)$ | α (sigmoid) | -18 | -13 | 1.8 |
| | | | | β (sigmoid) | 2 | 11 | 0.45 |
| | h | α/(α+β) | $1e^{-3}/(\alpha+\beta)$ | α (sigmoid) | -121 | 22 | 0.105 |
| | | | | β (sigmoid) | -55 | -11 | 0.065 |
| **Kas** | $m^2$ | α/(α+β) | 1/(α+β) | α (sigmoid) | 54 | -22 | 0.25 |
| | | | | β (sigmoid) | -100 | 35 | 0.05 |
| | h | 0.8+(α/(α+β)*0.2 | 1/(α+β) | α (sigmoid) | -95 | 16 | 2.5 |
| | | | | β (sigmoid) | 50 | -70 | 2 |
| **Krp** | $m^2$ | α/(α+β) | 1/(α+β) | α (exp) | - | 24 | 16 |
| | | | | β (exp) | - | -45 | 2.4 |
| | h | 0.87+(α/(α+β)*0.13 | 1/(α+β) | α (exp) | - | -100 | 0.01 |
| | | | | β (exp) | - | 18 | 0.4 |
| **CaL1.2** | m | sigmoid | *see table 2* | - | -8.9 | -6.7 | 1 |
| | h | 0.17+(sigmoid)*0.83 | 44.3ms | - | -55 | 8 | 1 |
| **CaL1.3** | m | sigmoid | *see table 2* | - | -40 | -5 | 1 |
| | h | sigmoid | 44.3ms | - | -37 | 5 | 1 |
| **CaN** | $m^2$ | sigmoid | *see table 2* | - | -3 | -8 | 1 |
| | h | 0.21+(sigmoid)*0.79 | 70ms | - | -74.8 | 6.5 | 1 |
| **CaR** | $m^3$ | sigmoid | 5.1ms | - | -29 | -9.6 | 1 |
| | h | sigmoid | *see table 2* | - | -33.3 | 17 | 1 |
| **CaT** | $m^3$ | sigmoid | *see table 2* | - | -63 | -8 | 1 |
| | h | sigmoid | *see table 2* | - | -84 | 5 | 1 |

**Table 1. Steady state equations**. Tau values in these tables are not temperature corrected (see methods for temperature correction values). Equations: sigmoid = rate/(1 + (exp ((V- vhalf)/slope))); exp = (rate)*(exp((V)/slope))

| Channel Name | mh form | tau | α or β equation | Rate* | Slope (mV) | Vhalf (mV) |
|---|---|---|---|---|---|---|
| **Naf** | $m^3$ | Eqn1 | - | 1.45 | 8 | -62 |
| | h | Eqn2 | - | 1.2 | 3 | -42 |
| **CaL1.2**§ | m | 1/(α+β) | α(linoid) | 39.8e3 | 8.124e-3 | 9.005e-3 |
| | | | β(exp) | 0.99e3 | 31.4e-3 | - |
| **CaL1.3**§ | m | 1/(α+β) | α(linoid) | 39.8e3 | 67.24e-3 | 15.005e-3 |
| | | | β(exp) | 3.5e3 | 31.4e-3 | - |
| **CaN**§ | $m^2$ | 1/(α+β) | α(linoid) | 39.8e3 | 17.19e-3 | 15.22e-3 |
| | | | β(exp) | 384.2 | 23.82e-3 | - |
| **CaR**§ | h | (1/(α+β))+20 | α(linoid) | 10e6 | 94.5e-3 | 5.12e-3 |
| | | | β(exp) | 84.2 | 13e-3 | - |
| **CaT** | $m^3$ | (1/(α+β))+2.2 | α(linoid) | 14.552e3 | 84.5e-3 | 7.12e-3 |
| | | | β(exp) | 4.9842e3 | 13e-3 | - |
| | h | (1/(α+β))+100 | α(linoid) | 2.652e3 | 94.5e-3 | 5.12e-3 |
| | | | β(exp) | 684.2 | 13e-3 | - |

**Table 2. Tau equations for inward currents.** Tau values in this table have not been temperature corrected (see methods for temperature correction values). Equations: Eqn1 = 0.1 + (rate/(1 + (exp ((V-vhalf)/slope))))^2; Eqn2 = 0.2754 + (rate/(1 + (exp ((V- vhalf)/slope)))); linoid : (rate*(V+vhalf))/((exp(V+vhalf))/slope)-1); exp: (rate*exp(V/slope)). *Rate units are $ms^{-1}$ for linoid and exp, and ms for eqn 1 and 2. § Channels undergoing CDI with the equation: $(0.0005^3/(0.0005^3+[Ca^{2+}]^3)^{100}$ and a time constant of 47.3ms, only when CDI is turned on.

| **Gbar ($S/M^2$)** | **soma** | **prox dend** | **mid dend** | **dist dend** |
|---|---|---|---|---|
| **NaF** | 50,000 | 6,000 | 6,000 | 2,000 |
| **Kir** | 11 | 11 | 11 | 11 |
| **KaF** | 300 | 550 | 550 | 550 |
| **KaS** | 200 | 22 | 22 | 22 |
| **Krp** | 14 | 14 | 14 | 14 |
| **SK** | 1 | 1 | 1 | 1 |
| **BK** | 10 | 10 | 10 | 10 |
| **Pbar (cm/s)** | | | | |
| **CaL1.2** | 6e-7 | 1e-7 | 1e-7 | 1e-7 |
| **CaL1.3** | 3e-7 | 0.5e-8 | 0.5e-8 | 0.5e-8 |
| **CaN** | 12e-7 | 0 | 0 | 0 |
| **CaR** | 8e-7 | 10e-7 | 10e-7 | 10e-7 |
| **CaT** | 0 | 0 | 8e-8 | 8e-8 |

**Table 3**. **Maximal conductance and permeability for ionic channels.** Gbar=maximal conductance $S/M^2$=Siemans per meter squared; Pbar = maximal calcium permeability cm/s=centimeters per second. Prox dend = proximal dendrites (up to 42µm from the soma); mid dend = middle dendrites (42µm-60µm from soma); dist dend = distal dendrites (60µm -224µm from soma).

| | Conc (μM) | Kf (/μM/s) | Kb (/s) | Diff ($(m^2)$/s) |
|---|---|---|---|---|
| **CaMN** | 15 | 100 | 1000 | 11e-12 |
| **CaMC** | 15 | 6 | 9.1 | 11e-12 |
| **Calbindin** | 80 | 28 | 19.6 | 0 |

888 **Table 4. Calcium buffer parameters.** CaMN= calmodulin N terminal binding site, CaMC= calmodulin C
889 terminal binding site. Conc: concentration; Diff: diffusion constant.

890

891

892

893

| | Gbar (pS) | $\tau_1$ (ms) | $\tau_2$ (ms) |
|---|---|---|---|
| **NMDA** | 470 | 2.2312 | 25 |
| **AMPA** | 171 | 1.1 | 5.75 |
| **GABA** | 900 | 0.25 | 3.75 |

894 **Table 5: conductances and time constants for synaptic channels.** Gbar is maximal conductance. Time
895 constants have already been temperature corrected by a qfactor of 2. $\tau_1$= activation time constant;
896 $\tau_2$=inactivation time constant.

897

898

899

900

| Input Name | Frequency for first10ms (Hz) | Frequency for middle 200ms (Hz) | Frequency for last 90ms (Hz) |
|---|---|---|---|
| **Flat** | 40 | 40 | 40 |
| **Gradient 1 (G1)** | 200 | 40 | 10 |
| **Gradient 2 (G2)** | 400 | 50 | 20 |
| **Gradient 3 (G3)** | 500 | 30 | 10 |
| **Gradient 4 (G4)** | 600 | 20 | 0 |

901 **Table 6: Input gradients used to create upstates.** Input frequencies for different input shapes. Input G3
902 was used for simulations unless otherwise specified. (see also figure 5)

903

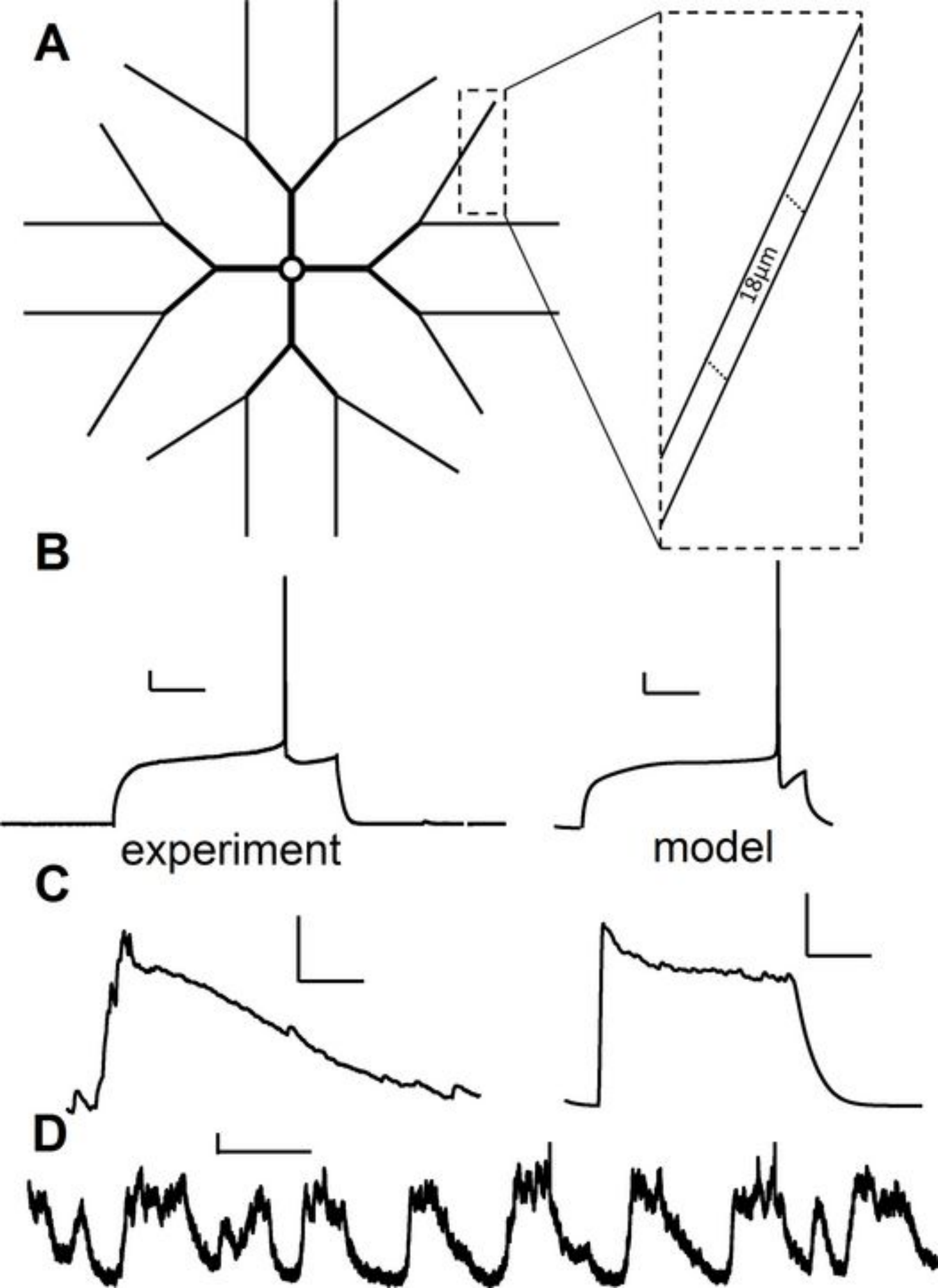
A
18µm
B
experiment
model
C
D

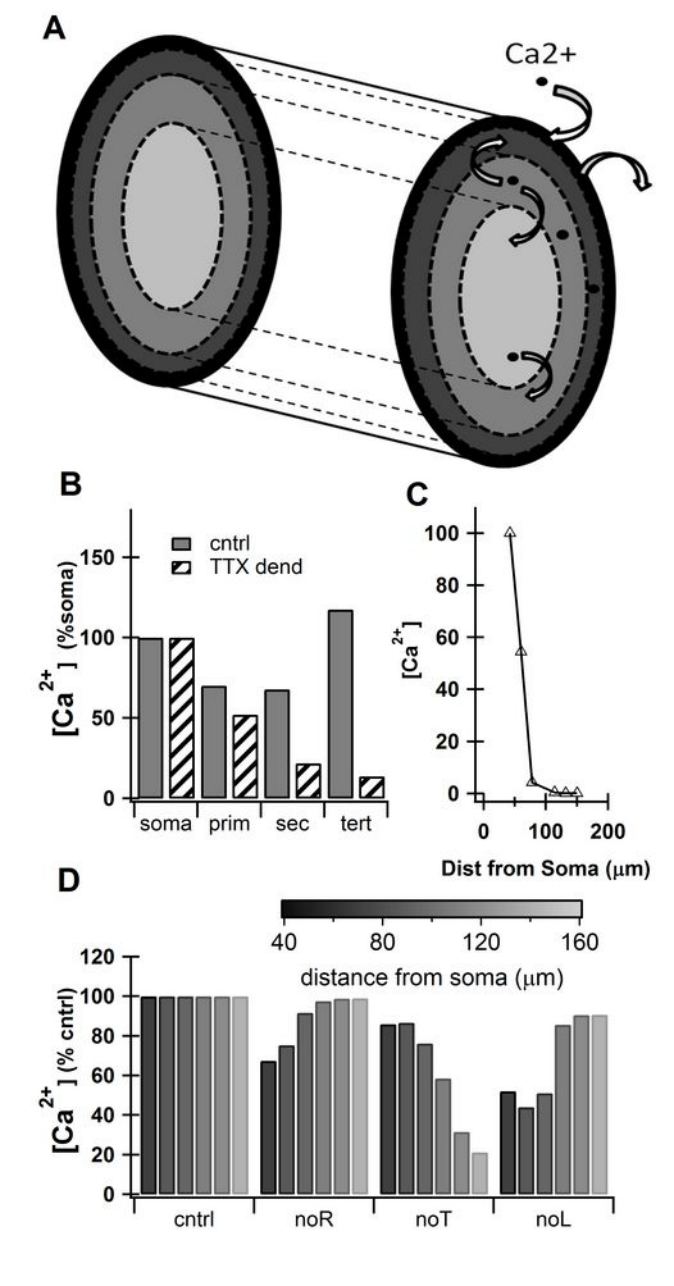
A
Ca2+
B
cntrl
TTX dend
[Ca2+] (%soma)
150
100
50
0
soma
prim
sec
tert
C
[Ca2+]
100
80
60
40
20
0
0
100
200
Dist from Soma (μm)
D
40
80
120
160
distance from soma (μm)
[Ca2+] (% cntrl)
120
100
80
60
40
20
0
cntrl
noR
noT
noL

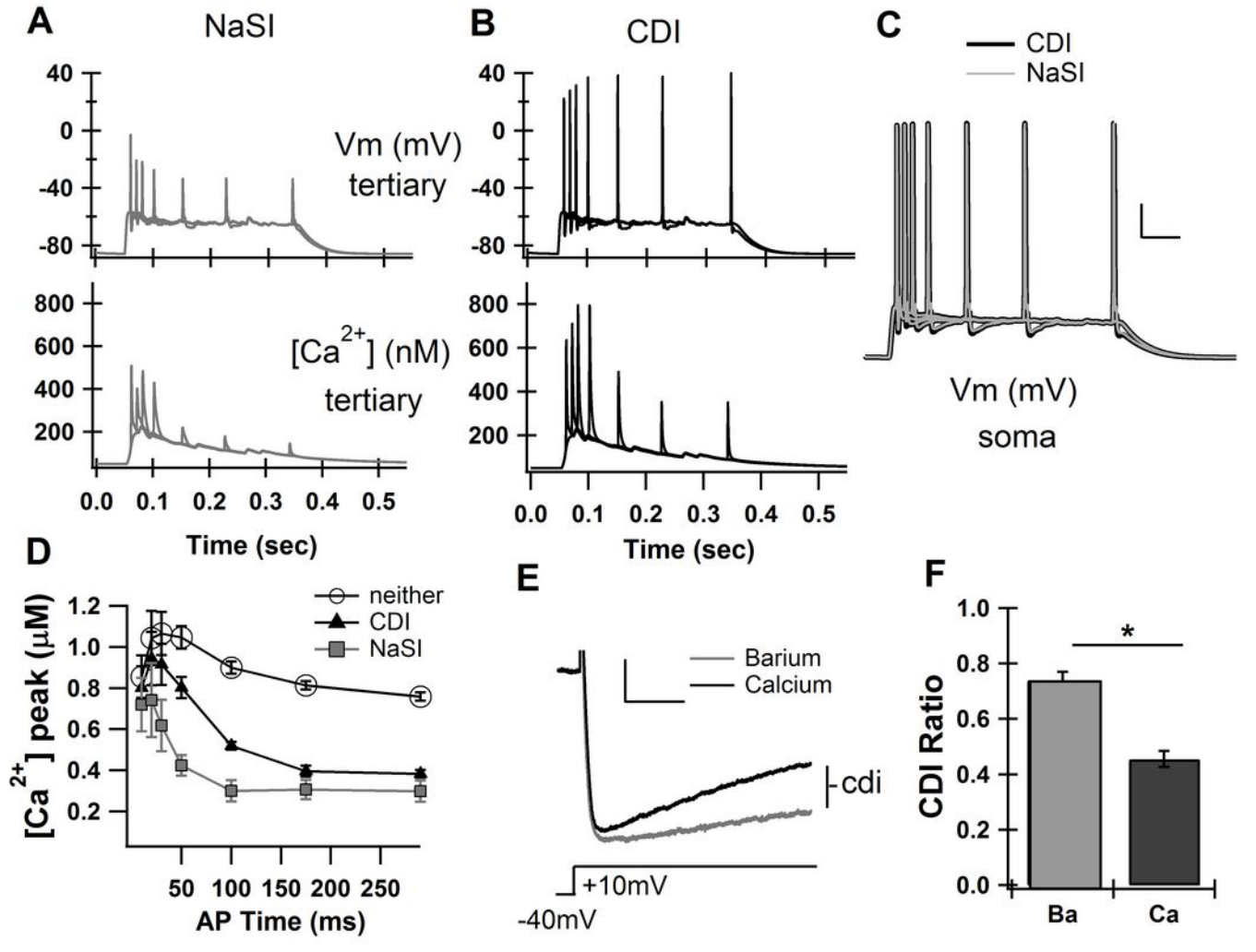
A
NaSI
B
CDI
C
CDI
NaSI
40
0
-40
-80
Vm (mV)
tertiary
800
600
400
200
[Ca2+] (nM)
tertiary
0.0 0.1 0.2 0.3 0.4 0.5
Time (sec)
Vm (mV)
soma
D
neither
CDI
NaSI
[Ca2+] peak (μM)
1.2
1.0
0.8
0.6
0.4
0.2
50 100 150 200 250
AP Time (ms)
E
Barium
Calcium
cdi
+10mV
-40mV
F
CDI Ratio
1.0
0.8
0.6
0.4
0.2
0.0
*
Ba
Ca

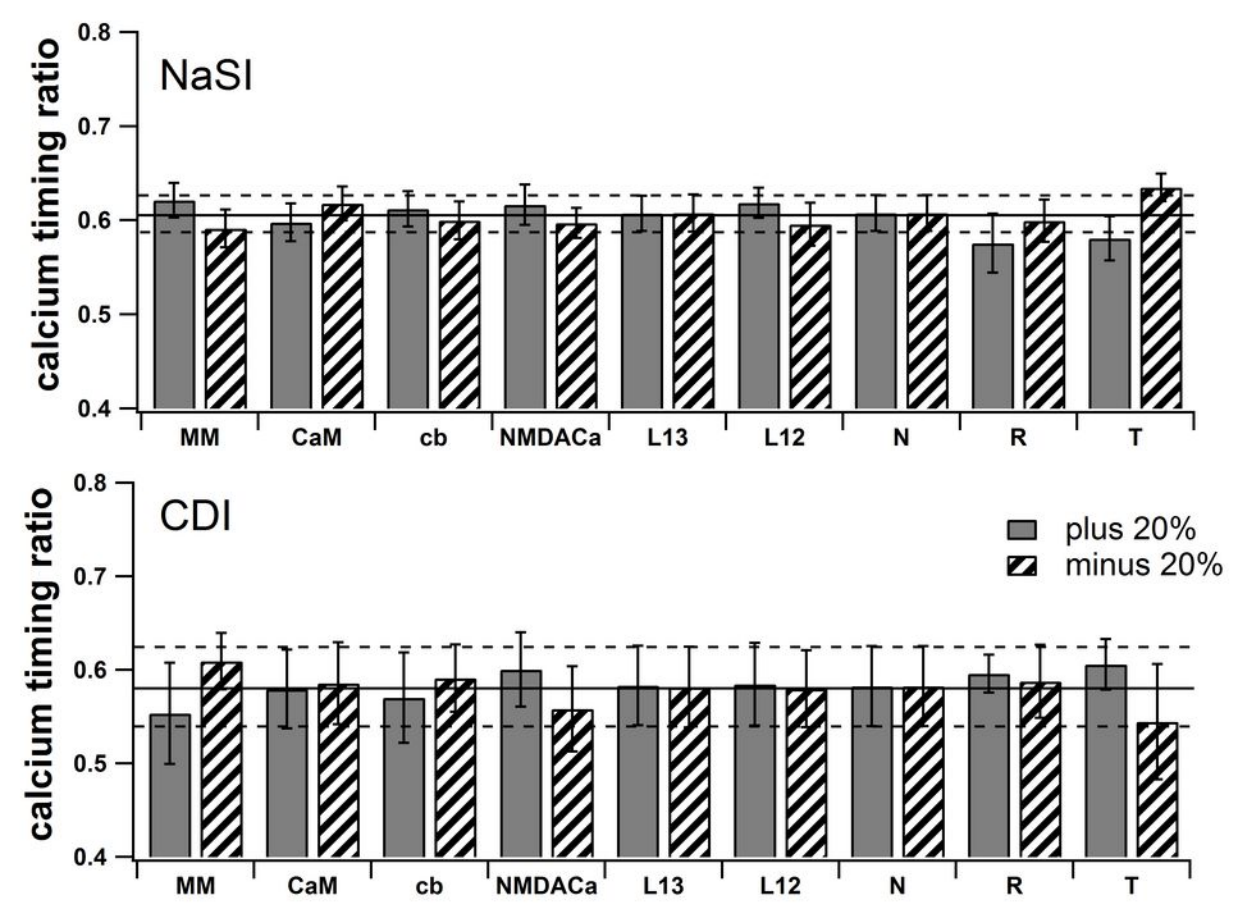
NaSI
calcium timing ratio
0.8
0.7
0.6
0.5
0.4
MM
CaM
cb
NMDACa
L13
L12
N
R
T
CDI
calcium timing ratio
plus 20%
minus 20%
0.8
0.7
0.6
0.5
0.4
MM
CaM
cb
NMDACa
L13
L12
N
R
T

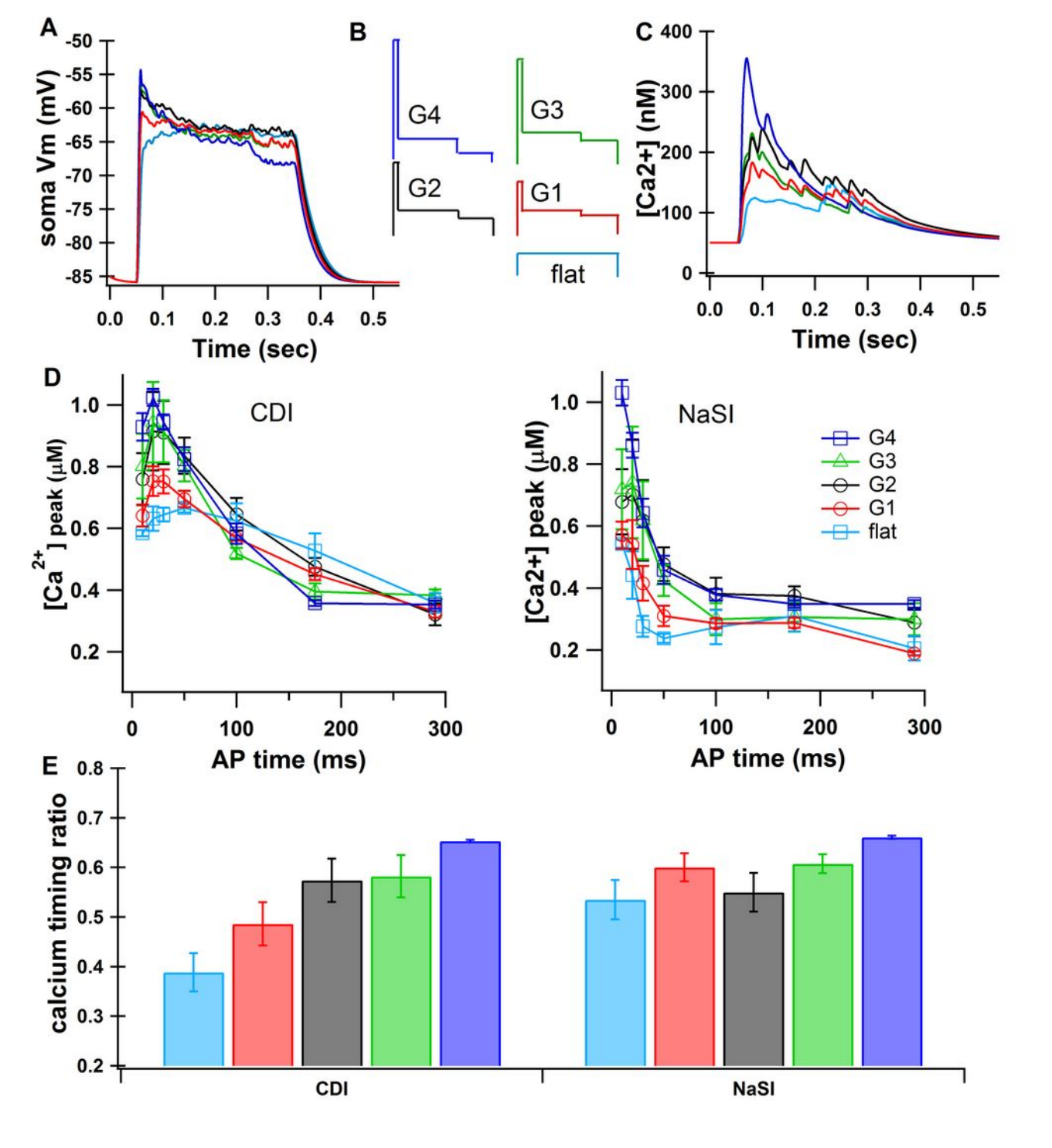
A
soma Vm (mV)
-50
-55
-60
-65
-70
-75
-80
-85
0.0
0.1
0.2
0.3
0.4
0.5
Time (sec)
B
G4
G3
G2
G1
flat
C
[Ca2+] (nM)
400
300
200
100
0
0.0
0.1
0.2
0.3
0.4
0.5
Time (sec)
D
CDI
[Ca2+] peak (μM)
1.0
0.8
0.6
0.4
0.2
0
100
200
300
AP time (ms)
NaSI
[Ca2+] peak (μM)
G4
G3
G2
G1
flat
1.0
0.8
0.6
0.4
0.2
0
100
200
300
AP time (ms)
E
calcium timing ratio
0.8
0.7
0.6
0.5
0.4
0.3
0.2
CDI
NaSI

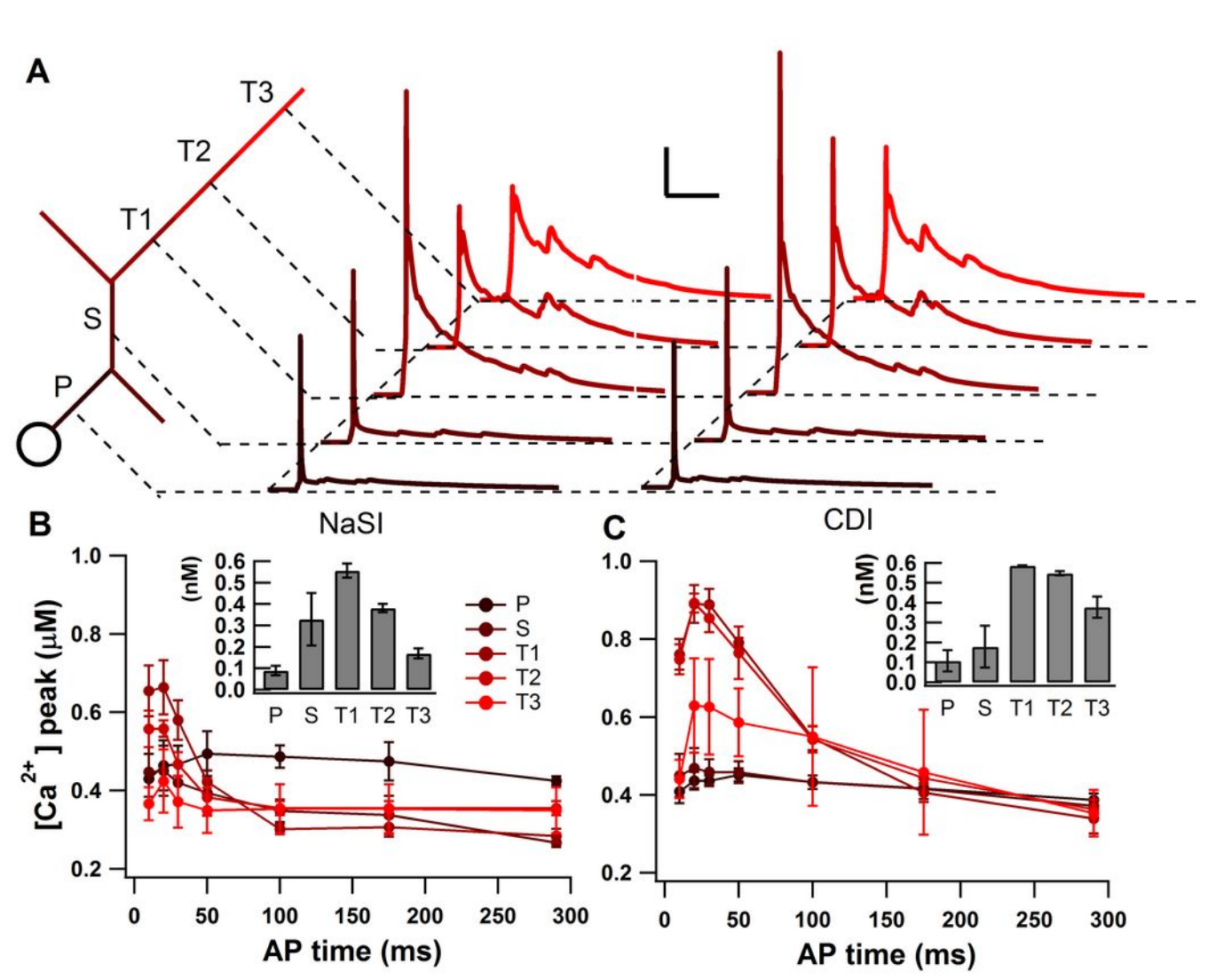
A
T3
T2
T1
S
P
B
NaSI
[Ca2+] peak (μM)
AP time (ms)
(nM)
P
S
T1
T2
T3
C
CDI
AP time (ms)

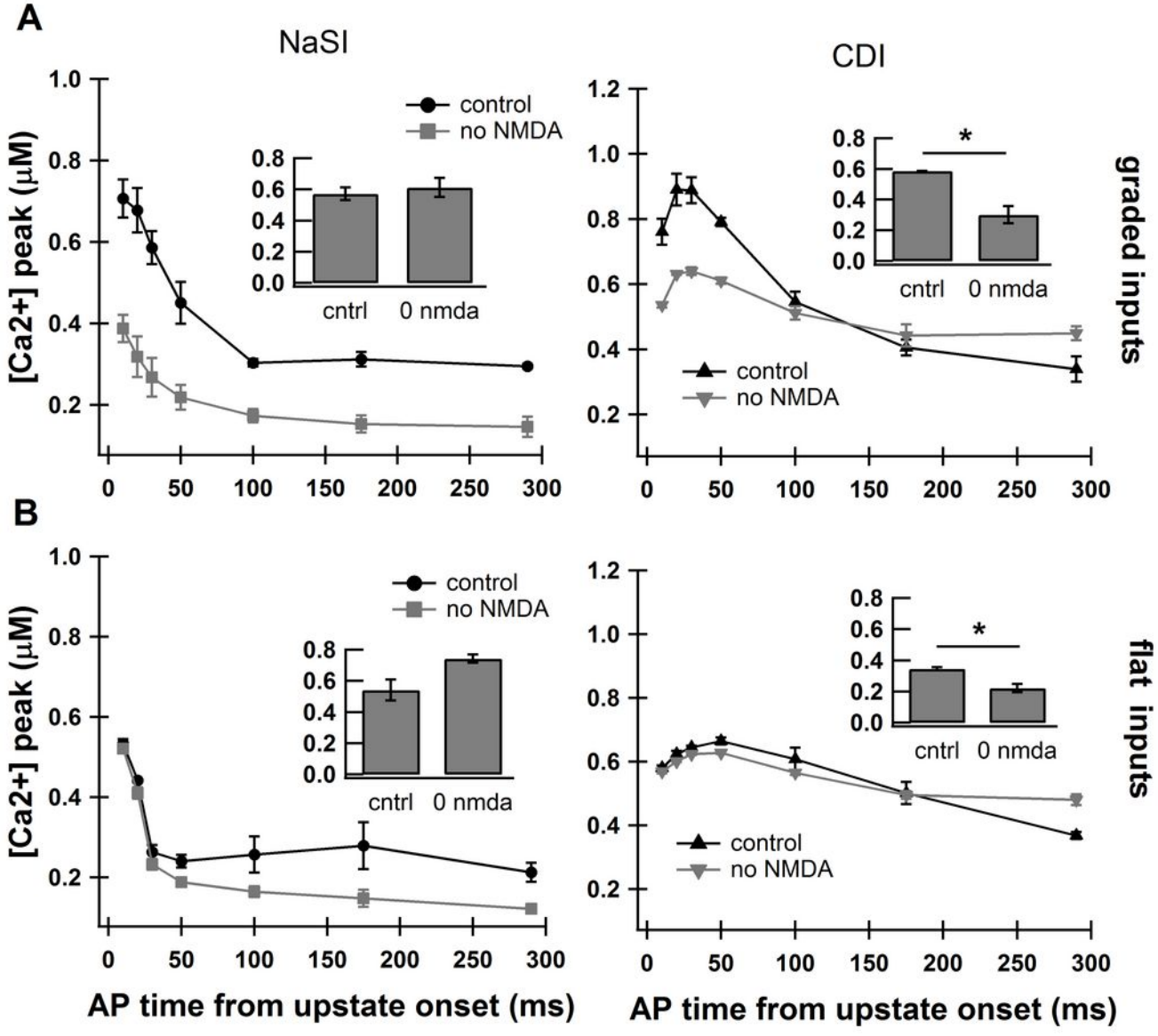
A
NaSI
CDI
graded inputs
[Ca2+] peak (μM)
control
no NMDA
cntrl
0 nmda
*
B
flat inputs
AP time from upstate onset (ms)

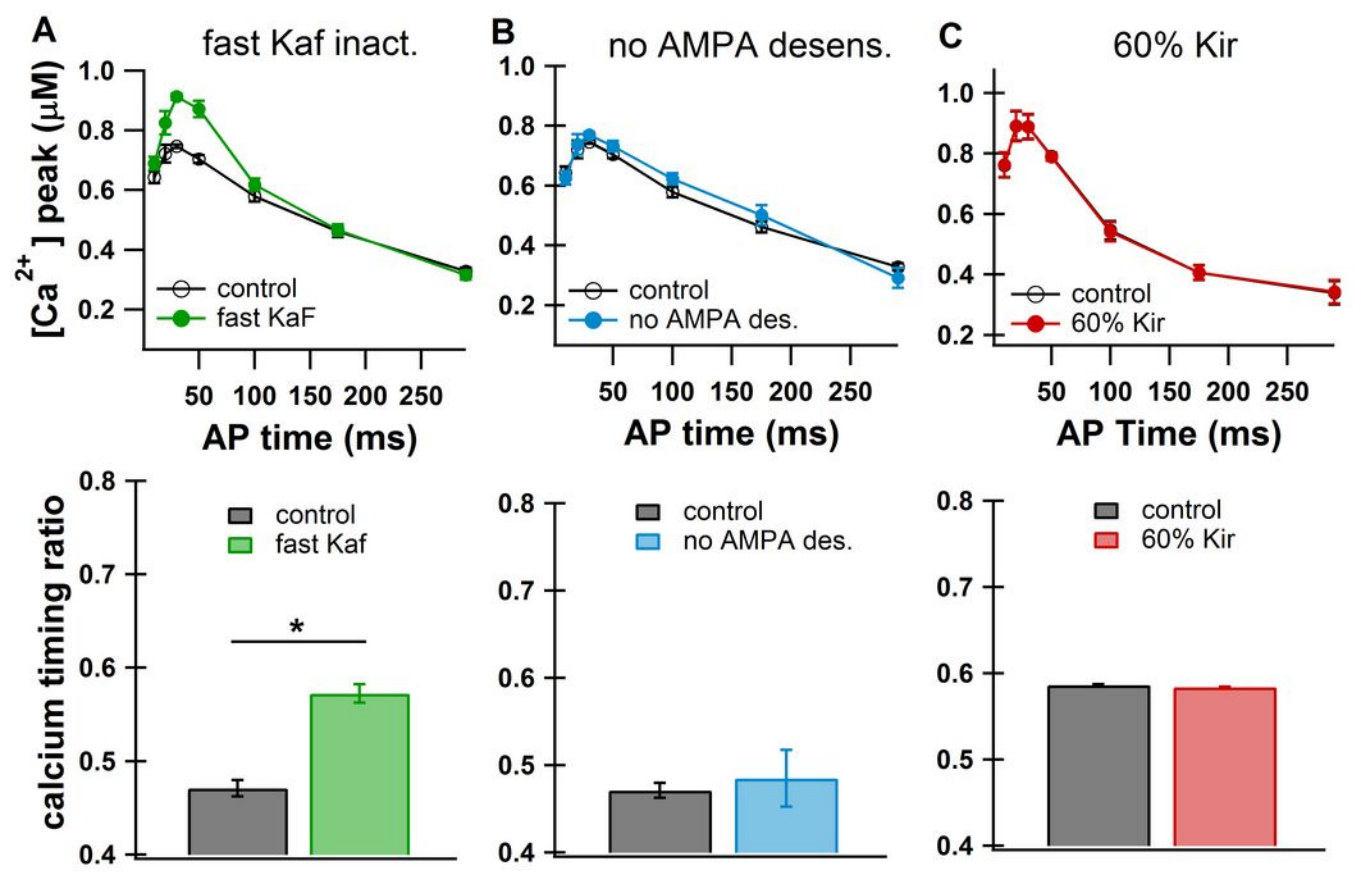
A
fast Kaf inact.
[Ca2+] peak (μM)
control
fast KaF
AP time (ms)
B
no AMPA desens.
control
no AMPA des.
AP time (ms)
C
60% Kir
control
60% Kir
AP Time (ms)
calcium timing ratio
control
fast Kaf
*
control
no AMPA des.
control
60% Kir

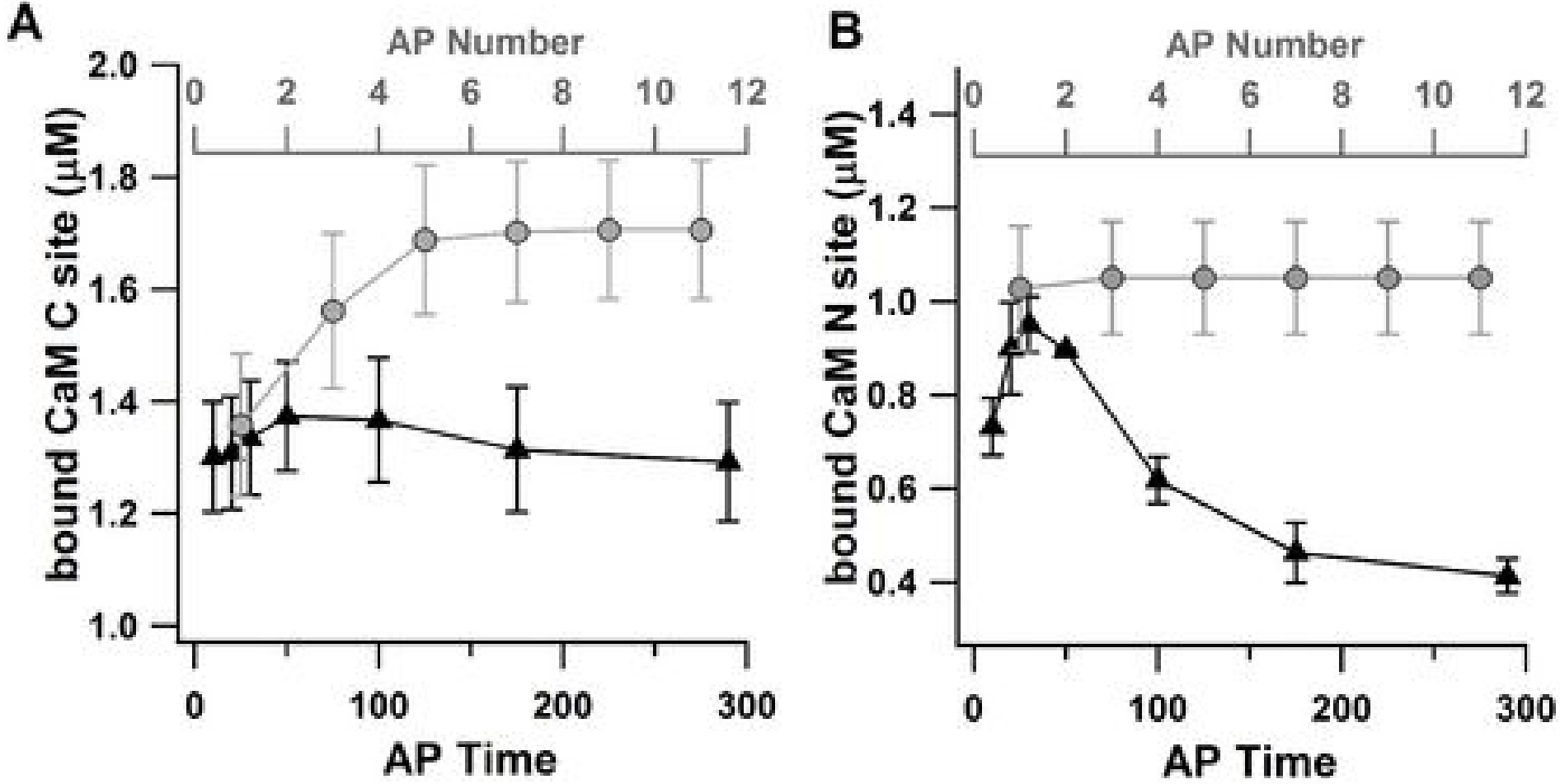
A
AP Number
0
2
4
6
8
10
12
2.0
1.8
1.6
1.4
1.2
1.0
bound CaM C site (μM)
0
100
200
300
AP Time
B
AP Number
0
2
4
6
8
10
12
1.4
1.2
1.0
0.8
0.6
0.4
bound CaM N site (μM)
0
100
200
300
AP Time

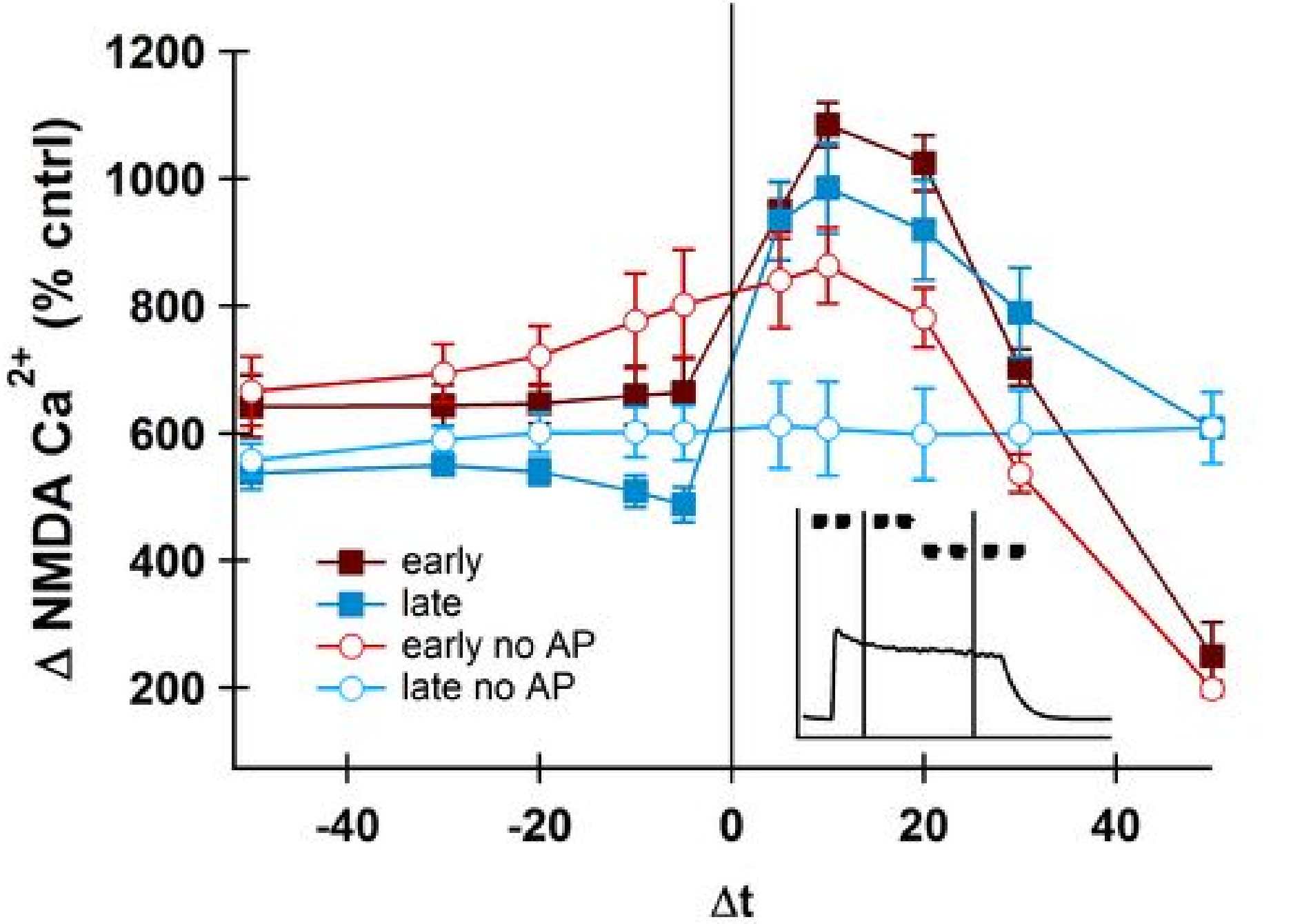
1200
1000
800
600
400
200
Δ NMDA Ca2+ (% cntrl)
early
late
early no AP
late no AP
-40
-20
0
20
40
Δt